geosciences

MDPI

Article

Geochemical and Isotopic Features of Geothermal Fluids Around the Sea of Marmara, NW Turkey

Francesco Italiano [1,2,*], Heiko Woith [3], Luca Pizzino [4], Alessandra Sciarra [4] and Cemil Seyis [5,†]

[1] OGS, Borgo Grotta Gigante 42/C, 34010 Sgonico, Italy
[2] Athanor-Geotech srls, via GregorioVII 396, 00165 Rome, Italy
[3] GFZ Helmholtz Centre for Geosciences, 14473 Potsdam, Germany; heiko.woith@gfz.de
[4] INGV Istituto Nazionale di Geofisica e Vulcanologia, Sezione di Roma 1, via di Vigna Murata 605, 00143 Rome, Italy; luca.pizzino@ingv.it (L.P.); alessandra.sciarra@ingv.it (A.S.)
[5] TÜBITAK Marmara Research Centre, Earth and Marine Science Institute, 41470 Gebze, Turkey; cemil.seyis@tubitak.gov.tr
* Correspondence: fitaliano@ogs.it
† Now at ALSELSAN.

Abstract: Investigations carried out on 72 fluid samples from 59 sites spread over the area surrounding the Sea of Marmara show that their geochemical and isotopic features are related to different segment settings of the North Anatolian Fault Zone (NAFZ). We collected fluids from thermal and mineral waters including bubbling and dissolved gases. The outlet temperatures of the collected waters ranged from 14 to 97 °C with no temperature-related geochemical features. The free and dissolved gases are a mixture of shallow and mantle-derived components. The large variety of geochemical features comes from intense gas–water (GWI) and water–rock (WRI) interactions besides other processes occurring at relatively shallow depths. CO_2 contents ranging from 0 to 98.1% and helium isotopic ratios from 0.11 to 4.43 Ra indicate contributions, variable from site to site, of mantle-derived volatiles in full agreement with former studies on the NAFZ. We propose that the widespread presence of mantle-derived volatiles cannot be related only to the lithospheric character of the NAFZ branches and magma intrusions have to be considered. Changes in the vertical permeability induced by fault movements and stress accumulation during seismogenesis, however, modify the shallow/deep ratio of the released fluids accordingly, laying the foundations for future monitoring activities.

Keywords: hydrogeochemistry; He and C isotopes; seismogenic process; NAFZ; Marmara

Academic Editor: Suzanne Golding

Received: 21 December 2024
Revised: 27 January 2025
Accepted: 7 February 2025
Published: 1 March 2025

Citation: Italiano, F.; Woith, H.; Pizzino, L.; Sciarra, A.; Seyis, C. Geochemical and Isotopic Features of Geothermal Fluids Around the Sea of Marmara, NW Turkey. *Geosciences* **2025**, *15*, 83. https://doi.org/10.3390/geosciences15030083

1. Introduction

It is well known that earthquakes may affect the fluid inventory co- and post-seismically with changes in water level in wells (Wang and Manga, 2010) [1], in temperature (Mogi et al., 1989) [2] and/or chemical composition (Skelton et al., 2014; Woith et al., 2003) [3,4], in the flow rate of gas discharges (Heinicke et al., 2006) [5] and in their chemical and isotopic composition (Hilton, 2007; Mutlu et al., 2012) [6,7].

The geodynamic (geological setting, tectonics, seismicity) context of the area deeply influences the composition and the behavior of the fluids in terms of both chemical and isotopic composition as shallow-originated fluids usually mix with fluids coming from different crustal levels and/or from the upper mantle. Such fluid mixing may change with time due to both seasonal variations and seismogenic processes (stress accumulation, deformation, strain release) [8]. As the fluids have high mobility migrating through

fractures and faults and are fast carriers of information on the physico-chemical conditions at depth, they are able to reveal modifications in the equilibrium conditions at depth.

This paper accounts for the gas and water geochemistry including thermal and cold waters as well as free and dissolved gases vented around the Sea of Marmara with the hope that the collected information will be the reference for the future design of continuous monitoring systems. Furthermore, any future changes in the geochemical features of the circulating fluids can be compared with those here presented and discussed. The knowledge of origin, provenance and role of the monitored fluids is necessary for the correct interpretation of any possible recorded temporal change.

2. Seismotectonics of the Marmara Region

The Marmara Sea region constitutes a transition zone between the strike-slip regime of the North Anatolian Fault (NAF) and the extensional regime of the Aegean Sea [9] (Bozkurt, 2001). NAF is a right-lateral strike-slip fault zone separating accreciated material of the Neo-Tethyan ocean (in the western part represented by the Sakarya continent) in the south from older and stiffer basement rocks to the north (Şengör et al., 2005) [10]. While the slip rate along the NAF increases from east to west from 17 to 25 mm/year (Reilinger et al., 2006; Tatar et al., 2012) [11,12], the locking depth decreases from 20 to 17 km (Duman et al., 2016) [13]. West of Bolu (about 31.5° E), the NAF splits into several fault strands separated by pull-apart sub-basins, so that the deformation becomes distributed. Both geological offsets (about 85 km over 5 Ma) as well as present-day motion derived from GPS measurements suggest that 70–90% of the total motion is taken up by the northern strand of the NAF (Armijo et al., 2002; Flerit et al., 2003; Karakaş et al., 2018) [14–16]. More than 40 earthquakes with magnitudes above M = 7 occurred in the past 2000 years within the wider Marmara region (Ambraseys and Finkel, 1991; Ambraseys, 2000; Ambraseys and Jackson, 2000; Ambraseys, 2002) [17–20] (see labelled white stars in Figure 1).

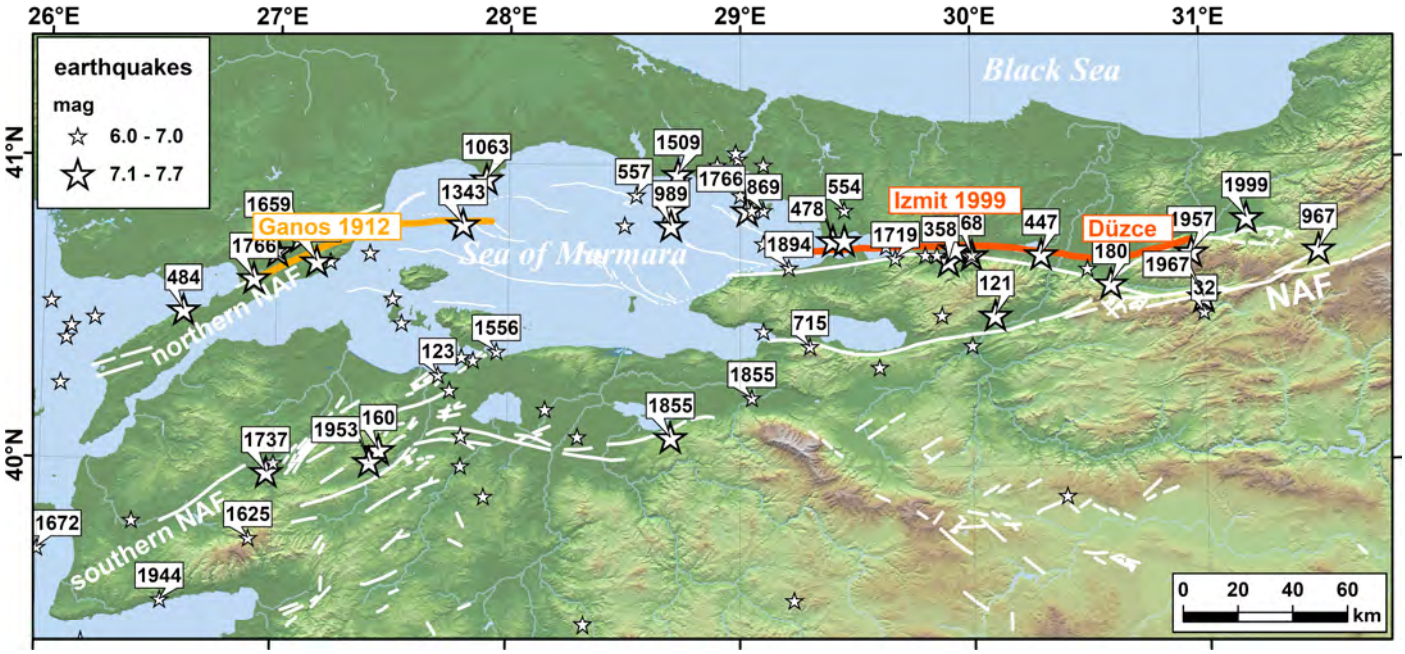

Figure 1. Map of historic earthquakes in the wider Marmara region compiled from various sources [17–20]. Labels indicate the year of the event for magnitudes M ≥ 7. White lines depict active faults according to the General Directorate of Mineral Research and Exploration (MTA) [21]; off-shore faults are taken from Armijo et al. (2002) [14]. Orange and red lines indicate the ruptures related to the Ganos earthquake of 1912 and the Izmit/Düzce events of 1999, respectively.

During the past century, a series of strong earthquakes migrated along the NAF from east to west (Stein et al., 1997) [22]. The last events in this series took place in 1999 and ruptured the Izmit and Düzce segments of the NAF with magnitudes of Mw = 7.4 and 7.2, respectively (Barka, 1999; Reilinger et al., 2000; Tibi et al., 2001) [23–25]. West of the Sea of Marmara, the last major earthquake occurred in 1912 (Mw = 7.2) along the Ganos fault (Ambraseys and Finkel, 1987) [26]. Thus, the Sea of Marmara constitutes a "seismic gap" (Polonia et al., 2004; Ergintav et al., 2014) [27,28].

Volcanic rocks occur widespread in the southwestern segment on the Biga peninsula. Magmatic activity started in early Miocene with calc-alkaline extrusive as well as intrusive rocks and ended in late Pliocene with alkaline rocks, predominantly basalts (Yilmaz, 1990) [29]. Due to intense seismo-tectonic faulting and tertiary volcanic activity, close to 100 thermal and mineral springs have formed south of the Marmara Sea (Şimşek, 1997) [30]. This is in clear contrast to the area north of the NAF where very few low temperature thermal springs occur. Also, very few earthquakes occurred during the past century and active faults have not been mapped in the oil- and gas-rich (Hoşgörmez and Yalçın, 2005) [31] Thrace basin (Duman et al., 2016) [13]. The lack of deep-reaching fault systems might explain the absence of thermal springs.

An average terrestrial surface heat flow of 60 mW/m^2 was determined by Pfister et al. (1998) [32]. High heat flow values (80–110 mW/m^2) occur south of the Marmara Sea corresponding to an extensional tectonic regime, whereas normal values (60–72 mW/m^2) were found north of the Sea of Marmara. The authors noted that the occurrence of thermal springs does not coincide with heat flow density. Instead, they are controlled by active tectonics with large thermal springs occurring preferentially in trans-tensional regimes. The combination of strike-slip and normal faults seem to promote elevated vertical hydraulic permeability within the crust.

Previous studies on the water and gas geochemistry of mineral and thermal waters as well as their isotopic signatures were carried out for the following areas (the locations are shown in Figure A1, Appendix A): Eskişehir (Yüce et al., 2017) [33], Kuzuluk (Balderer et al., 1991; Greber, 1994) [34,35]; Armutlu (Eisenlohr, 1997) [36]; Oylat (Pasvanoğlu, 2011) [37]; Bursa (Imbach, 1997; Tut Haklidir, 2013) [38,39]; Ekşidere (Yalcin, 1997) [40]; Biga peninsula (Mutlu, 2007; Yalcin, 2007 [41]; Sanliyuksel and Baba, 2011) [40–43]; Tuzla/Çanakkale (Mützenberg, 1997; Baba et al., 2009) [44,45]. Regional studies on noble gases were provided by Doğan et al., 2009 [46]. Gas emissions located in the deep offshore are CH_4-dominated, and were extensively studied during the past 15 years (Geli et al., 2018) [47].

3. Materials and Methods

During two field campaigns in 2013 and 2014 carried out over an area 78,000 km^2, a suite of 72 fluid samples including bubbling and free gases as well as cold and thermal waters were collected from 59 sites of natural springs, fountains (türkish: *Çeşme*) and thermal and cold ponds located around the Sea of Marmara (Figure 2).

In the field, measurements of water temperature, pH, redox potential (Eh) and electrical conductivity (EC) were performed with multi-parameter devices (HACH HQ40D with electrodes). Samples for major cation and anion analyses were filtered using a 0.45 µm nylon filter, and stabilized with ultrapure HNO_3. Table 1 lists the full sample suite including coordinates, elevation above the sea level, field data and information on the types of samples. Details on the laboratory techniques and procedures to determine the geochemical features in terms of chemical and isotopic composition of waters and gases (including dissolved and bubbling gas phase) are reported in Appendix B.

Table 1. Sampling sites (listed in alphabetical order of investigated areas shown in Figure 2) around the Sea of Marmara. Geographic coordinates in decimal degrees, altitude above sea level (mNN) and indications on the location types (*Çesme*—fountain) are reported besides the field data of water temperature (wT in °C), electrical conductivity (EC in µS/cm at 25 °C), pH, Eh_{SHE} (mV), and dissolved oxygen (mg/L). The presence of bubbling gases is also reported (gas). Kapl.—*Kaplıcası* (bath); MS—*Maden Suyu* (mineral water). For sample locations see Figure 2.

ID	Lon	Lat	mNN	Area	Site	Type	Date	wT	EC	pH	Eh_{SHE}	Oxy	Gas
1	26.8857	39.5894	11	Balıkesir	Edremit Güre IGJ-1	well 167 m	03.09.2014	50.7	1114	8.59	28	1.2	
2	27.5614	40.0295	250	Balıkesir	Ekşidere	spring	03.09.2014	37.9	373	7.39	162	2.1	
3	27.5790	40.0050	225	Balıkesir	Ekşidere "Gencli Su"	Çesme	03.09.2014	19.3	198	3.87	461	2.5	
4	27.7719	39.8761	130	Balıkesir	Ilica (Balya)	spring	29.05.2013	55.4	1193	8.12	189		x
5	28.1330	40.0939	20	Balıkesir	Ilicaboğazi Susurluk	spring	30.05.2013	58.6	3170	6.70			
							04.09.2014	53.0	3340	6.73		1.7	
6	27.9106	40.0654	34	Balıkesir	Kızık (Manyas)	well 30 m	30.05.2013	51.1	1807	6.64	241		
7	31.5189	40.6746	821	Bolu	Çepni Aci Su	spring	04.06.2013	21.5	1957	6.16	429	0.3	x
8	31.2414	40.7212	423	Bolu	Derdin	spring	04.06.2013	30.5	8180	6.67	118	1.1	x
9	31.0279	40.7607	136	Bolu	Efteni Kapl.	spring	04.06.2013	42.5	3130	6.40	59	0.1	x
10	31.0074	40.5987	572	Bolu	Ilica (Taşkesti)	well	05.06.2013	59.8	1410	8.70	44		
11	31.2401	40.4591	1044	Bolu	Mudurnu Babas	well 125 m, artes.	05.06.2013	38.1	1186	6.43	214	0.7	
12	31.2398	40.4595	1055	Bolu	Mudurnu Babas NW	well 250 m, artes.	05.06.2013	39.4	1178	6.52	139	1.9	x
13	31.2414	40.4604	1063	Bolu	Mudurnu Babas NE	well 400 m, artes.	05.06.2013	40.2	1174	6.37	184	0.1	
14	29.0183	40.2001	224	Bursa	Çekirge Vakifbahce	spring	30.05.2013	46.1	567	6.96	241		
							04.09.2014	46.5	601	7.04	342	1.2	
15	29.0368	40.1989	143	Bursa	Kükürtlü Uni Hospital	spring	03.06.2013	64.3	1407	6.65	224		
							08.09.2014	62.9	1430	6.84	−21	3.9	
16	29.0404	40.1985	127	Bursa	Kükürtlü BK2	well 400 m, artes.	03.06.2013	18.5	1305	7.65	−26	0.1	x
							08.09.2014	25.7	1141	8.24	−286	0.3	x
17	29.0466	40.1973	135	Bursa	Kükürtlü BJ-3	well 750 m, artes.	03.06.2013	16.5	667	8.29	−56	1.9	
18	29.0795	40.0403	566	Bursa	Çaybaşi Uludağ MS	well 32 m	05.09.2014	22.2	2179	6.37	152	3.9	
19	29.0884	40.0372	590	Bursa	Çaybaşi Özkaynak MS	spring	08.09.2014	20.1	1307	6.08	213	3.3	
20	29.5863	39.9274	711	Bursa	Oylat Eski Hamam	spring	10.06.2013	40.7	735	7.38	394	4.2	
21	29.6715	40.0128	465	Bursa	Özlüce "Suyu Çesme"	Çesme	10.06.2013	15.8	2510	6.22	254	1.5	
22	29.6510	40.0100	358	Bursa	Kınık Maden Suyu	well	10.06.2013	14.5	2300	6.46	294	3.6	
23	29.6489	40.0151	353	Bursa	Kınık Maden Suyu N	well, artesian	10.06.2013	17.2	6510	6.58	179	0.2	x
24	29.6362	40.0181	370	Bursa	Çitli (Inegöl)	Çesme	10.06.2013	19.7	7980	6.70	134	0.1	x
25	29.5900	40.3708	298	Bursa	Yk. Gölüce "Tuzlu Su"	Çesme	02.06.2013	16.8	3580	7.47	−56	5.7	
26	29.4766	40.4980	109	Bursa	Keramet Ilica	spring in lake	02.06.2013	31.9	902	6.75	444	1.0	x

Table 1. *Cont.*

ID	Lon	Lat	mNN	Area	Site	Type	Date	wT	EC	pH	Eh_{SHE}	Oxy	Gas
27	29.4452	40.4977	86	Bursa	Çakırlı CH_4-Çesme	well 86 m	02.06.2013	18.3	580	7.78		0.0	x
28	29.3089	40.4679	102	Bursa	Orhangazi Ilıpinar	spring in lake	02.06.2013	17.0	666	7.01	364	6.7	
29	29.1604	40.4234	5	Bursa	Gemlik Merkez Kapl.	well, artesian	03.06.2013	36.2	425	7.42	232	5.3	
30	28.4315	39.9487	75	Bursa	Dümbüldek	well, artesian	30.05.2013	50.6	2520	6.38	165		
31	28.4295	39.9526	67	Bursa	Dümbüldek spring	spring	30.05.2013	16.3	2930	6.05	204		x
							04.09.2014	19.4	3050	6.29	131	2.4	x
32	28.3894	39.9964	59	Bursa	Yalıntaş Aci Su	Çesme	04.09.2014	19.5	2133	6.14	411	0.3	
33	26.1916	39.7449	33	Çanakkale	Kestanbol	well	02.09.2014	75.7	31580	6.28	99	2.8	
34	26.1788	39.5677	39	Çanakkale	Tuzla	spring	02.09.2014	97.0	93000	6.74	109	3.9	x
35	27.2413	40.0923	195	Çanakkale	Kirkgecit Kapl.	spring	29.05.2013	52.1	662	9.03	24		x
36	26.9745	39.9169	181	Çanakkale	Bardakçılar Dağ Kapl.	spring	29.05.2013	50.7	1608	8.18	264		x
37	27.1557	39.8442	296	Çanakkale	Yenice Hıdırlar Kapl.	spring	29.05.2013	82.7	955	7.50	131		x
							03.09.2014	83.2	1073	8.08	−18	4.1	x
38	30.1680	39.8143	859	Eskişehir	Inönü Ilica	spring	09.06.2013	27.4	431	7.51	384	5.8	
39	30.5198	39.7738	790	Eskişehir	Eskişehir Hamamyolu	well	09.06.2013	45.7	498	7.40	319	3.3	
40	31.0376	39.6878	817	Eskişehir	Uyushamam E-8	well 45 m	08.06.2013	15.6	1814	5.99	389	1.0	x
41	31.0600	39.6794	800	Eskişehir	Uyushamam	spring	08.06.2013	28.3	1275	6.44	209	0.5	x
42	31.7223	39.4423	921	Eskişehir	Hamamkarahisar Çardak	spring	08.06.2013	35.0	768	7.13	224	3.6	
43	29.2948	40.8449	3	Istanbul	Tuzla "Büyük Içmeler"	well 158 m, artes.	31.08.2014	20.4	14740	6.86	359		
44	29.8773	40.6975	28	Kocaeli	Yeniköy	well, artesian	04.06.2013	31.5	381	9.10	−36	1.1	
45	29.8772	40.6967	37	Kocaeli	Yeniköy Jazlik Ilica	spring	04.06.2013	29.7	372.4	8.98	89		
46	30.6477	40.6210	111	Sakarya	Kuzuluk W	well	31.08.2014	19.6	8020	6.54	134	3.3	x
47	30.6570	40.6257	127	Sakarya	Kuzuluk K-3	well 160 m	31.08.2014	72.0	3750	6.89	−11	1.8	x
48	30.3632	40.4715	412	Sakarya	Ahibaba Ilık Su	spring	05.06.2013	24.9	2210	6.29	239	0.8	x
49	30.4282	40.3989	415	Sakarya	Taraklı	well, artesian	05.06.2013	42.5	948	6.62	104	1.6	
50	27.2596	40.7355	221	Tekirdağ	Hoşköy Özkaynak MS	spring	01.09.2014	18.2	3810	6.80	49	1.4	
51	27.2125	40.7128	242	Tekirdağ	Yayaköy (Şarköy)	Çesme	28.05.2013	14.1	14800	6.95	−164		
52	27.1064	40.6847	158	Tekirdağ	Gölcük	Çesme	28.05.2013	14.9	4150	7.11	−111		
							01.09.2014	15.8	2510	7.36	−1	1.1	
53	28.8400	40.5457	76	Yalova	Armutlu kapl.	well	31.05.2013	74.6	2640	6.23	174		x
54	28.8431	40.5465	87	Yalova	Armutlu IPA2	well 500 m							x
55	28.8432	40.5465	82	Yalova	Armutlu spring	spring	01.06.2013	58.8	2600	6.40	64		
56	28.8402	40.5455	78	Yalova	Armutlu near bridge	well, artesian	01.06.2013	75.6	3010	6.29	69		x
57	29.2778	40.5939	178	Yalova	Soğucak Aci Su	spring	31.05.2013	21.4	1119	6.75	365		
58	29.1712	40.6038	132	Yalova	Termal "Göz Suyu"	Çesme	31.05.2013	59.7	1870	7.57	174		
59	29.1705	40.6039	136	Yalova	Termal Kapl.	spring	31.05.2013	63.4	1820	7.35	49		

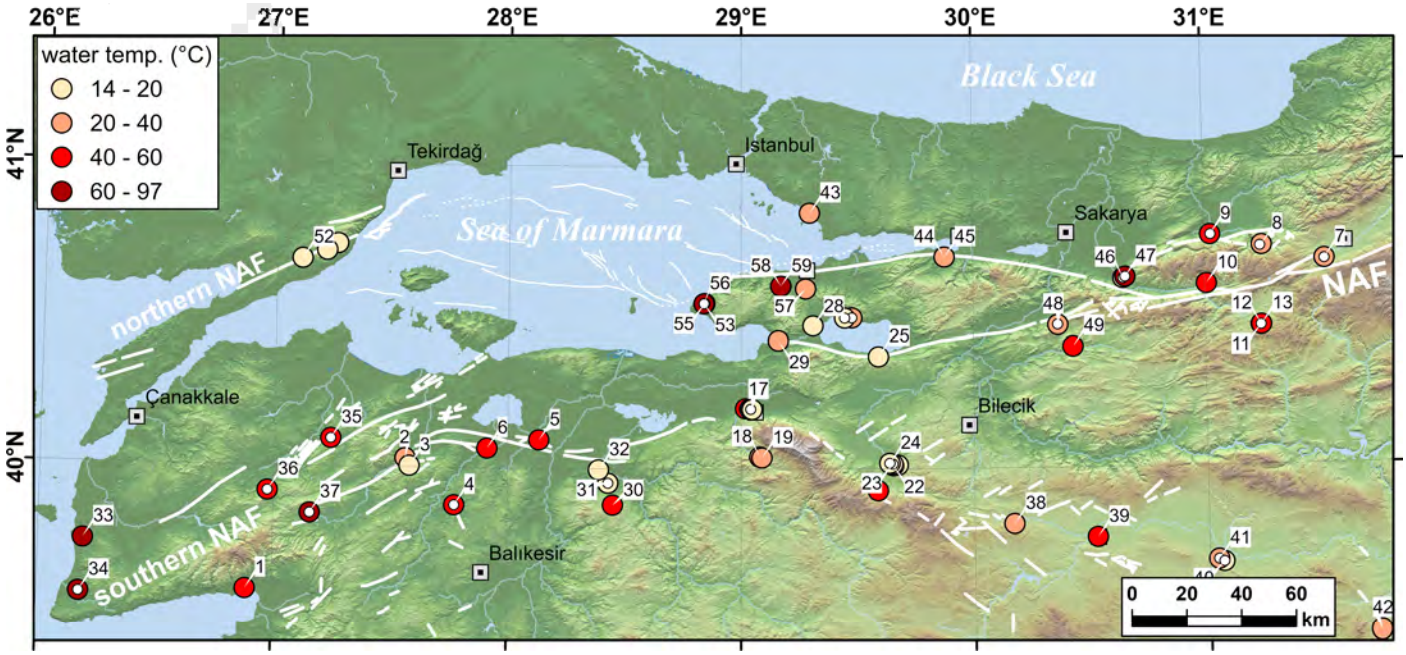

Figure 2. Map of fluid sampling sites around the Sea of Marmara. Symbols indicate color-coded water temperatures. Small white circles depict sites with bubbling gases. Values are sample numbers used in this study (see Table 1). Names of geographic areas investigated are given.

4. Results

Data for water composition are listed in Table 2. Table 3 lists the analytical results of the dissolved gases and Table 4 those of the bubbling gases. All data are available in electronic form at the GFZ data archive https://dataservices-cms.gfz-potsdam.de/ (accessed on 1 February 2025) where additional information is provided about the errors of the isotope measurements.

Table 2. Water geochemistry. The chemical and isotopic composition of the water samples are listed, pCO_2 in bars, ion concentrations in meq/L, isotopic ratios in δ ‰ vs SMOW. The sea water composition is taken by https://www.britannica.com/science/seawater (accessed on 1 February 2025). See text for water-type classification. Empty cells = below detection limits; n.a. = not analyzed.

ID	Site	Date	pCO_2	Li	Na	K	Mg	Ca	F	Cl	NO_3	SO_4	HCO_3	$\delta^{18}O$	$\delta^{2}H$	Water Type
1	Edremit	03.09.2014	0.03	0.04	9.64	0.28	0.01	0.75	0.37	2.07	0.01	7.13	1.20	−6.79	−47.00	Na-SO_4
2	Ekşidere	03.09.2014	0.13		0.45	0.05	0.90	2.39	0.02	0.21		0.35	3.20	−9.12	−59.00	Ca-HCO_3
3	Ekşi.Genc	03.09.2014			0.50	0.04	0.15	0.70	0.00	0.42		0.92	0.05	−8.97	−51.00	acid-SO_4
4	Ilica (Balya)	29.05.2013	0.05	0.10	10.40	0.12	0.01	0.84	0.40	2.51	0.16	7.23	1.57	−10.25	−70.16	Na-SO_4
5	Ilicaboğazi	30.05.2013	0.44	0.10	25.97	0.43	1.83	4.16	0.05	21.21	0.01	2.03	9.97	−9.23	−58.71	Na-Cl
		04.09.2014	0.40	0.07	24.15	0.49	1.69	4.17	0.05	19.78	0.06	1.89	9.10	−9.32	−58.00	Na-Cl
6	Kızık	30.05.2013	0.46	0.15	11.70	0.73	0.95	6.79	0.03	8.39	0.01	1.84	10.94	−8.17	−55.48	Na(Ca)-HCO_3(Cl)
7	Çepni	04.06.2013	0.68	0.04	1.10	0.10	2.97	21.60	0.01	0.44	0.08	0.05	25.55	−11.10	−75.72	Ca-HCO_3
8	Derdin	04.06.2013	0.81	0.20	81.82	1.11	5.81	7.17	0.77	9.49	0.01	26.32	62.94	−8.39	−70.63	Na-Cl
9	Efteni	04.06.2013	0.79	0.13	16.02	0.31	12.41	7.17	0.04	4.47		0.01	31.38	−11.08	−75.16	Na(Mg)-HCO_3
10	Ilica (Taşk.)	05.06.2013	0.02	0.04	7.66	0.11	0.07	5.82	0.05	0.32		13.39	0.38	−13.11	−88.17	Na(Ca)-SO_4
11	Mudurnu	05.06.2013	0.53	0.04	0.96	0.15	4.15	9.02	0.06	0.17		0.57	14.10	−11.87	−78.98	Ca(Mg)-HCO_3
12	Mudur NW	05.06.2013	0.51	0.04	0.94	0.15	4.16	8.69	0.06	0.13		0.59	13.82	−11.61	−77.67	Ca(Mg)-HCO_3
13	Mudurnu NE	05.06.2013	0.57	0.04	0.99	0.15	4.34	9.15	0.06	0.11		0.62	14.55	−11.71	−78.36	Ca(Mg)-HCO_3

Table 2. *Cont.*

ID	Site	Date	pCO_2	Li	Na	K	Mg	Ca	F	Cl	NO_3	SO_4	HCO_3	$\delta^{18}O$	$\delta^{2}H$	Water Type
14	Çekirge	30.05.2013	0.27	0.01	1.25	0.11	1.73	4.13	0.04	0.13		1.22	6.10	−10.94	−70.34	Ca-HCO_3
		04.09.2014	0.23	0.01	1.49	0.22	1.81	3.28	0.82	0.15	0.01	1.19	4.90	−10.72	−71.00	Ca-HCO_3
15	Kükürtlü Uni	03.06.2013	0.49	0.12	9.66	0.48	0.78	4.96	0.24	0.32	0.05	5.63	10.55	n.a.	n.a.	Na(Ca)-$HCO_3(SO_4)$
		08.09.2014	0.39	0.09	8.88	0.50	0.70	4.51	0.24	0.34	0.01	5.55	8.70	−9.79	−71.00	Na(Ca)-$HCO_3(SO_4)$
16	Kükürtlü BK2	03.06.2013	0.16	0.13	9.96	0.52	0.65	2.41	0.24	0.29	0.01	2.05	11.78	−10.81	−71.08	Na-HCO_3
		08.09.2014	0.09	0.10	10.65	0.57	0.68	1.07	0.23	0.31		0.55	12.00	−10.51	−77.00	Na-HCO_3
17	Kükürtlü BJ-3	03.06.2013	0.06	0.05	6.16	0.15	0.69	1.07	0.02	0.09		1.18	6.45	−10.38	−67.71	Na-HCO_3
18	Çaybaşi UMS	05.09.2014	0.58	0.47	8.16	0.78	6.21	9.62	0.12	2.51	0.12	0.64	21.80	−8.78	−65.00	Ca(Mg)-HCO_3
19	Çaybaşi ÖMS	08.09.2014	0.55	0.14	2.92	0.26	9.47	4.31	0.04	0.99	0.01	0.68	15.40	−9.26	−61.00	Mg(Ca)-HCO_3
20	Oylat	10.06.2013	0.14	0.04	0.97	0.12	0.68	6.51	0.03	0.16	0.02	4.97	3.49	−10.78	−69.65	Ca-$SO_4(HCO_3)$
21	Özlüce	10.06.2013	0.67	0.11	11.40	0.38	11.37	9.75	0.02	0.66		1.28	30.23	−11.16	−75.50	Na(Mg)-HCO_3
22	Kınık	10.06.2013	0.57	0.15	14.32	0.56	5.96	9.90	0.02	0.70	0.06	0.99	27.82	−11.10	−76.11	Na(Ca)-HCO_3
23	Kınık N	10.06.2013	0.82	0.46	65.54	2.69	5.75	10.04	0.01	1.86		2.05	73.43	−12.06	−89.28	Na-HCO_3
24	Çitli (Inegöl)	10.06.2013	0.88	0.47	90.32	1.12	6.41	12.86	0.02	1.73		2.03	98.94	−11.76	−88.60	Na(HCO_3)-Cl
25	Yk. Gölüce	02.06.2013	0.13	0.08	36.14	0.44	1.76	1.54	0.37	32.83	0.05	2.22	4.95	−10.80	−73.73	Na-Cl
26	Keramet	02.06.2013	0.38	0.04	1.15	0.05	2.89	7.67	0.02	0.37	0.01	0.58	11.37	−10.19	−65.02	Ca(Mg)-HCO_3
27	Çakırlı	02.06.2013	0.11	0.04	2.61	0.04	1.42	3.42	0.01	0.62		0.03	7.02	−12.37	−81.31	Ca(Mg)-HCO_3
28	Orhangazi	02.06.2013	0.23		0.43	0.03	0.46	7.36		0.35	0.34	0.43	7.48	−9.54	−59.18	Ca-HCO_3
29	Gemlik	03.06.2013	0.15	0.00	0.51	0.03	1.28	3.26	0.01	0.47	0.03	0.23	4.50	−10.22	−63.22	Ca-HCO_3
30	Dümbüldek	30.05.2013	0.82	0.16	18.61	1.72	2.26	7.93	0.08	1.63		0.11	29.03	−10.50	−68.49	Na(Ca)-HCO_3
31	Dümb. spr.	30.05.2013	0.77	0.16	16.52	1.53	3.93	16.73	0.06	1.72		1.68	35.50	−10.47	−68.39	Na(Ca)-HCO_3
		04.09.2014	0.68	0.13	15.72	1.47	3.60	14.85	0.04	1.74	0.01	1.77	31.00	n.a.	n.a.	Na(Ca)-HCO_3
32	Yalıntaş	04.09.2014	0.63	0.13	12.14	1.21	2.67	8.37	0.09	1.68	0.01	1.16	21.70	−10.73	−76.00	Na(Ca)-HCO_3
33	Kestanbol	02.09.2014	0.48	2.45	271.3	18.13	5.24	43.23	0.48	336.7	0.35	3.70	5.00	−6.69	−40.00	Na-Cl
34	Tuzla	02.09.2014	0.09	2.74	547.0	33.10	4.10	97.31		660.0	0.25	2.27	0.15	n.a.	n.a.	Na-Cl
35	Kirkgecit	29.05.2013	0.02	0.02	6.36	0.05	0.01	0.26	0.43	1.23	0.05	3.44	1.83	−9.72	−61.35	Na-SO_4
36	Bardakcilar	29.05.2013	0.04	0.05	12.70	0.17	0.02	4.21	0.29	0.86		15.32	0.94	−9.49	−61.63	Na(Ca)-SO_4
37	Hidirlar	29.05.2013	0.12	0.05	7.88	0.17	0.02	0.87	0.36	0.46		6.83	1.66	−8.32	−51.30	Na-SO_4
		03.09.2014	0.06	0.01	8.06	0.20	0.01	0.85	0.38	0.47	0.01	7.12	1.20	n.a.	n.a.	Na-SO_4
38	Inönü Ilica	09.06.2013	0.13	0.04	0.37	0.02	1.79	2.93	0.01	0.11	0.10	0.10	4.92	−11.13	−75.57	Ca-HCO_3
39	Eskişehir	09.06.2013	0.17	0.04	0.62	0.04	2.67	2.47	0.01	0.18	0.05	0.28	5.36	−10.25	−72.82	Mg(Ca)-HCO_3
40	Uyush. E-8	08.06.2013	0.63	0.06	6.97	0.19	4.79	11.53	0.02	1.65	0.12	0.51	21.35	−10.91	−79.95	Ca(Mg)-HCO_3
41	Uyushamam	08.06.2013	0.49	0.04	1.79	0.21	7.77	6.75	0.02	0.61	0.01	0.95	14.28	−10.11	−72.02	Mg(Ca)-HCO_3
42	H.karahisar	08.06.2013	0.24		1.82	0.09	1.74	5.25	0.01	1.02	0.07	0.36	7.56	−10.68	−73.82	Ca-HCO_3
43	Tuzla Içmeler	31.08.2014	0.22		104.0	2.05	25.36	17.67		130.8	0.13	12.84	5.10	n.a.	n.a.	Na-Cl
44	Yeniköy	04.06.2013	0.02	0.04	3.33	0.01	0.04	0.30	0.03	1.09		0.69	1.92	−9.92	−63.21	Na-HCO_3
45	Yenik. Jazlik	04.06.2013	0.02	0.04	3.12	0.01	0.03	0.29	0.02	0.77	0.01	0.67	2.14	−9.77	−62.45	Na-HCO_3
46	Kuzuluk W	31.08.2014	0.82	0.72	74.21	2.47	9.82	10.69		32.83	0.02	0.58	65.00	3.56	−44.00	Na-Cl
47	Kuzuluk K-3	31.08.2014	0.63	0.37	30.28	1.07	1.19	4.73	0.23	9.71	0.01	1.16	26.80	−9.07	−86.00	Na-HCO_3
48	Ahibaba	05.06.2013	0.53	0.07	13.44	0.46	1.25	2.50	0.04	0.56		1.24	15.33	−10.87	−70.64	Na-HCO_3
49	Taraklı	05.06.2013	0.41	0.04	1.15	0.11	1.65	6.87	0.04	0.21		0.33	9.49	−11.66	−77.14	Ca-HCO_3
50	Hoşköy ÖMS	01.09.2014	0.58	0.12	42.08	0.39	2.22	2.79	0.13	1.60	0.01	0.21	45.30	n.a.	n.a.	Na-HCO_3

Table 2. *Cont.*

ID	Site	Date	pCO_2	Li	Na	K	Mg	Ca	F	Cl	NO_3	SO_4	HCO_3	$\delta^{18}O$	$\delta^{2}H$	Water Type
51	Yayaköy	28.05.2013	0.23	0.11	136.6	0.47	10.06	6.36	0.07	132.6	0.53	5.92	7.40	−8.80	−56.91	Na-Cl
52	Gölcük	28.05.2013	0.21	0.04	25.54	0.13	6.79	9.74	0.04	29.63		6.24	8.06	−8.08	−51.51	Na(Ca)-Cl
		01.09.2014	0.16		14.82	0.16	5.05	5.21	0.06	10.60	0.02	7.97	6.70	−8.33	−50.00	Na(Ca)-Cl
53	Armutlu	31.05.2013	0.64	0.21	15.32	0.75	1.81	14.88	0.11	7.50		17.13	9.19	−10.81	−69.62	Na(Ca)-SO_4
55	Armutlu spr.	01.06.2013	0.53	0.19	13.35	0.64	1.84	13.20	0.09	6.44	0.01	14.35	9.16	−10.46	−67.18	Na(Ca)-SO_4
58	Termal Göz	31.05.2013	0.24	0.01	0.45	0.06	2.76	11.26	0.01	0.24		0.30	14.67	−9.84	−60.63	Ca-HCO_3
59	Termal	31.05.2013	0.11	0.05	11.93	0.11	0.04	8.45	0.10	2.43		16.64	1.26	−11.23	−70.72	Na(Ca)-SO_4
	Iznik Lake	02.06.2013			4.70	0.30	5.50	0.60		1.90		0.60	8.40			
	Sea water				464.3	10.11	105.1	20.44		539.7	0.83	55.83	0.45			

Table 3. Chemical composition of the dissolved gases. Data in ccSTP/L_{H2O}. Total volume in milliliters of gas per liter of water. Empty cells indicate values below detection limits. Carbon isotopic composition of TDIC in δ ‰ vs PDB. Empty cells = below detection limits; n.a. = not analyzed.

ID	Site	Date	He	Ne	H_2	O_2	N_2	CO	CH_4	CO_2	Vol.	$\delta^{13}C_{TDC}$	N_2/O_2	He/Ne	R/Ra
1	Edremit	03.09.2014	7.8×10^{-4}	3.0×10^{-4}	2.5×10^{-4}	6.0	18.4	2.7×10^{-5}	3.0×10^{-2}	0.4	24.8	n.a.	3	2.59	2.60
2	Ekşidere	03.09.2014	1.3×10^{-4}	3.0×10^{-4}		6.0	18.2	7.0×10^{-6}		5.1	29.2	−1.45	3	0.43	0.43
3	Ekşi. Gencli	03.09.2014	8.9×10^{-5}	2.9×10^{-4}	4.8×10^{-4}	4.5	17.3		4.0×10^{-1}	70.3	92.5	n.a.	4	0.30	0.30
5	Ilicaboğazi	30.05.2013	2.9×10^{-4}	3.3×10^{-4}	8.4×10^{-4}	7.0	19.6	7.3×10^{-5}	2.5×10^{-3}	73.3	100.0	1.52	3	0.87	0.95
		04.09.2014	1.3×10^{-3}	2.4×10^{-4}	1.1 × 10-3	5.9	21.5	6.4×10^{-5}	2.1×10^{-3}	78.2	105.5	−0.85	4	5.30	1.00
6	Kizik	30.05.2013	1.3×10^{-3}	3.3×10^{-4}		1.3	13.7	6.9×10^{-6}	1.1×10^{-3}	85.4	100.4	−3.43	10	3.85	0.52
10	Ilica	05.06.2013	4.3×10^{-4}	3.6×10^{-4}	5.3×10^{-5}	1.4	6.0	1.4×10^{-5}	5.9×10^{-2}	0.0	7.5	n.a.	4	1.17	0.63
11	Mudurnu	05.06.2013	1.0×10^{-4}	2.1×10^{-4}		0.3	4.1			70.3	74.7	n.a.	14	0.51	1.41
13	Mudurnu NE	05.06.2013	3.5×10^{-4}	2.8×10^{-4}		0.4	2.9	7.3×10^{-6}		52.0	55.4	n.a.	7	1.25	1.85
14	Çekirge	30.05.2013	1.6×10^{-4}	3.8×10^{-4}		2.2	11.0	1.3×10^{-5}	2.5×10^{-3}	12.3	25.6	0.64	5	0.41	1.19
		04.09.2014	4.6×10^{-4}	2.4×10^{-4}		5.3	16.1		3.1×10^{-3}	17.6	39.0	−3.19	3	1.90	0.53
15	Kükürtlü Uni	03.06.2013	2.6×10^{-4}	2.8×10^{-4}		1.5	45.4		6.6×10^{-5}	53.1	100.0	0.04	31	0.94	0.67
		08.09.2014	4.5×10^{-4}	3.5×10^{-4}		8.0	30.3		5.5×10^{-2}	78.2	116.6	0.48	4	1.26	0.57
16	Kükürtlü BK2	03.06.2013	3.0×10^{-3}	1.8×10^{-4}		0.1	32.7		$1.6 \times 10^{+0}$	65.5	100.0	n.a.	649	16.6	1.05
		08.09.2014	5.2×10^{-3}	2.3×10^{-4}		5.2	20.6	2.2×10^{-5}	6.7×10^{-4}	4.2	30.0	2.91	4	22.3	0.43
17	Kükürtlü BJ-3	03.06.2013	2.3×10^{-4}	3.2×10^{-4}	1.8×10^{-4}	0.5	4.0		2.5×10^{-4}	0.8	5.3	n.a.	7	0.72	0.67
18	Çaybaşi UMS	05.09.2014	1.3×10^{-4}	1.1×10^{-4}		5.8	12.8	2.5×10^{-5}		525.4	544	2.84	2	1.19	0.84
19	Çaybaşi ÖMS	08.09.2014	2.4×10^{-4}	2.4×10^{-4}		9.3	22.8	1.6×10^{-5}		539.9	572	1.91	2	1.04	0.92
20	Oylat	10.06.2013	6.7×10^{-4}	2.3×10^{-4}	1.7×10^{-5}	0.6	2.5	4.1×10^{-6}		1.2	4.3	n.a.	4	2.93	0.70
21	Özlüce	10.06.2013	1.0×10^{-4}	2.3×10^{-4}	1.1×10^{-2}	0.4	0.7	4.5×10^{-6}	3.4×10^{-5}	246.6	248	n.a.	2	0.43	0.95
22	Kınık	10.06.2013	1.4×10^{-4}	2.8×10^{-4}	1.6×10^{-3}	0.5	2.6		3.7×10^{-4}	116.0	119.0	n.a.	6	0.49	0.78
25	Yk. Gölüce	02.06.2013	8.5×10^{-5}	2.0×10^{-4}								n.a.		0.42	0.86
28	Orhangazi	02.06.2013	1.1×10^{-4}	3.0×10^{-4}	8.5×10^{-5}	1.4	4.1			11.3	16.7	n.a.	3	0.38	0.97
29	Gemlik	03.06.2013	9.0×10^{-5}	2.6×10^{-4}		0.7	3.2	6.8×10^{-6}	9.8×10^{-5}	2.1	6.0	n.a.	4	0.35	0.94
30	Dümbüldek	30.05.2013	1.0×10^{-4}	2.3×10^{-4}		1.3	3.0	5.2×10^{-5}	4.2×10^{-3}	221.9	226	−6.47	2	0.43	1.12
31	Dümbüldek sp.	30.05.2013	1.1×10^{-4}	3.0×10^{-4}		5.6	11.0	1.0×10^{-4}	4.2×10^{-4}	2742	2759	0.67	2	0.35	1.15
		04.09.2014	1.3×10^{-4}	1.1×10^{-4}		5.8	12.8	2.5×10^{-5}		525.4	544	n.a.	2	1.19	0.84
32	Yalıntaş	04.09.2014	5.3×10^{-3}	1.1×10^{-4}		17.5	42.9		9.2×10^{-3}	936.7	997	3.52	2	49.7	0.90
33	Kestanbol	02.09.2014	5.2×10^{-3}	2.8×10^{-4}	1.3×10^{-3}	8.7	32.2	5.3×10^{-4}	2.1×10^{-1}	125.7	167	−1.71	4	18.2	0.87
37	Yenice Hidirlar	03.09.2014	7.8×10^{-4}	3.0×10^{-4}	2.5×10^{-4}	6.0	18.4	2.7×10^{-5}	3.0×10^{-2}	0.4	24.8	−13.86	3	2.59	0.47
38	Inönü	09.06.2013	1.2×10^{-4}	3.2×10^{-4}	1.3×10^{-4}	0.9	2.5	4.2×10^{-6}		1.4	4.9	n.a.	3	0.36	0.95
39	Eskişehir	09.06.2013	1.3×10^{-4}	2.9×10^{-4}	9.2×10^{-3}	0.8	3.1			1.7	5.7	n.a.	4	0.44	0.91
42	Hamam. Çardak	08.06.2013	4.3×10^{-4}	1.2×10^{-3}	3.2×10^{-4}	0.6	3.2	2.7×10^{-6}		6.5	10.2	n.a.	6	0.36	0.87
43	Tuzla Içmeler	31.08.2014	1.7×10^{-3}	1.5×10^{-4}	7.7×10^{-4}	7.3	19.0	4.0×10^{-5}		14.6	40.9	n.a.	3	11.4	0.59
44	Yeniköy	04.06.2013	6.3×10^{-3}	3.8×10^{-4}	1.2×10^{-3}	0.2	4.5	3.3×10^{-6}		0.0	4.7	n.a.	19	16.9	0.74
45	Yeniköy Jazlik	04.06.2013	1.4×10^{-3}	3.5×10^{-4}		0.4	3.7	1.7×10^{-6}	3.2×10^{-5}	0.0	4.2	n.a.	8	4.12	0.53
46	Kuzuluk W	31.08.2014	2.1×10^{-3}	8.6×10^{-5}								n.a.		24.3	0.64
47	Kuzuluk K-3	31.08.2014	1.6×10^{-4}	3.0×10^{-4}	4.2×10^{-3}	6.9	20.0		3.9×10^{-2}	101.0	127.9	n.a.	3	0.52	0.63

Table 3. *Cont.*

ID	Site	Date	He	Ne	H_2	O_2	N_2	CO	CH_4	CO_2	Vol.	$\delta^{13}C_{TDC}$	N_2/O_2	He/Ne	R/Ra
49	Tarakli	05.06.2013	1.4×10^{-4}	2.6×10^{-4}		0.9	3.4	3.1×10^{-6}	1.5×10^{-5}	21.1	25.4	n.a.	4	0.53	0.68
50	Hoşköy ÖMS	01.09.2014	3.2×10^{-4}	1.2×10^{-4}		0.1	12.5			320.8	333	n.a.	228	2.75	4.43
51	Yayaköy	28.05.2013	7.7×10^{-5}	1.8×10^{-4}		8.1	28.2	4.2×10^{-5}	5.5×10^{-0}	63.9	105.6	n.a.	3	0.43	2.08
52	Gölcük	28.05.2013	8.3×10^{-5}	2.5×10^{-4}		0.03	8.2	1.2×10^{-5}	2.7×10^{-0}	12.3	23.2	−17.47	238	0.34	0.94
		01.09.2014	6.1×10^{-5}	2.0×10^{-4}		2.9	14.7	1.6×10^{-4}		18.7	36.3	n.a.	5	0.31	0.76
53	Armutlu kapl.	31.05.2013	1.2×10^{-4}	4.1×10^{-4}		0.6	1.9	1.0×10^{-5}	8.7×10^{-2}	29.9	32.5	−3.73	3	0.29	0.87
55	Armutlu spring	01.06.2013	6.1×10^{-4}	3.2×10^{-4}	2.1×10^{-4}	0.7	2.0	2.1×10^{-6}		39.7	42.4	n.a.	3	1.91	0.34
58	Termal Göz	31.05.2013	1.4×10^{-4}	2.2×10^{-4}		2.1	6.7	1.3×10^{-5}	7.4×10^{-5}	18.4	27.2	n.a.	3	0.65	0.70
59	Termal	31.05.2013	1.3×10^{-3}	3.4×10^{-4}		1.4	6.1	3.5×10^{-6}		0.3	7.8	n.a.	4	4.00	0.34
	ASW		4.8×10^{-5}			4.8	9.6		1.0×10^{-6}	2.4	16.8		2		

Table 4. Chemical composition of the bubbling gases. Data in vol%. ^{40}Ar in ppm by vol. Carbon isotopic ratios in δ ‰ vs. PDB. Helium isotopic ratios expressed as R/Ra (see text). $\delta^{13}C$ values refer to CO_2.Empty cells indicate values below detection limits; n.a. = not analyzed.

Site	Date	He	Ne	H_2	O_2	N_2	CO	CH_4	CO_2	$\delta^{13}C$	He/Ne	R/Ra	^{40}Ar	$^{40}/^{36}Ar$	$CO_2/^3He$
Ilica Çamur	29.05.2013	6.7×10^{-4}	1.9×10^{-3}	4.4×10^{-8}		95.3		2.4×10^{-1}	2.7	−17.2	0.36	0.97	1.8	298.6	2.9×10^{9}
Çepni	04.06.2013	7.0×10^{-4}	1.9×10^{-3}		1.7	6.6	2.0×10^{-5}	3.2×10^{-4}	91.5	−1.8	0.37	0.95	0.2	300.5	9.9×10^{10}
Derdin	04.06.2013	4.1×10^{-4}	4.1×10^{-4}		0.3	1.6	4.0×10^{-5}	3.3×10^{-3}	98.1	−4.2	1.00	0.72	n.a.	n.a.	2.4×10^{11}
Efteni	04.06.2013	6.6×10^{-4}	1.8×10^{-3}	1.3×10^{-7}	0.0	1.4	1.8×10^{-5}	8.0×10^{-1}	97.8	−3.3	0.37	0.98	n.a.	n.a.	1.1×10^{11}
Mudurnu NW	05.06.2013	1.1×10^{-3}	1.5×10^{-3}	9.0×10^{-8}	13.7	62.1		1.4×10^{-2}	23.4	−5.2	0.78	1.60	0.9	298.8	9.2×10^{9}
Lues refer to COKükürtlü BK2	03.06.2013			6.1×10^{-3}		33.5	4.3×10^{-4}	1.2×10^{0}	65.2	−5.2	n.a.	n.a.	n.a.	n.a.	
Kınık N	10.06.2013	5.9×10^{-3}	1.9×10^{-4}		0.1	2.4	2.0×10^{-5}	1.1×10^{-3}	97.4	−3.7	30.8	0.52	0.1	296.2	2.3×10^{10}
Çitli	10.06.2013	1.1×10^{-2}	1.0×10^{-3}		0.4	4.8		3.9×10^{-3}	94.5	−6.2	10.1	0.52	0.3	301.9	1.2×10^{10}
Keramet	02.06.2013	2.7×10^{-3}	2.1×10^{-3}		2.0	82.3	3.0×10^{-5}	3.1×10^{-3}	15.7	−9.4	1.28	0.47	n.a.	n.a.	8.9×10^{9}
Çakırlı	02.06.2013	6.5×10^{-4}	2.0×10^{-3}			8.9		9.1×10^{1}	0.1	−14.3	0.32	0.97	n.a.	n.a.	1.5×10^{8}
Dümbüldek sp.	30.05.2013	1.7×10^{-4}	4.2×10^{-4}		1.6	4.5	3.0×10^{-5}	9.6×10^{-3}	93.9	−5.0	0.40	0.98	n.a.	n.a.	4.1×10^{11}
Dümbüldek sp.	04.09.2014	1.0×10^{-3}	6.4×10^{-5}		1.7	5.3	1.1×10^{-4}	2.6×10^{-2}	93.0	n.a.	15.5	1.18	n.a.	n.a.	5.7×10^{10}
Tuzla	02.09.2014	1.4×10^{-3}	2.9×10^{-5}		0.5	1.5	9.0×10^{-4}	2.1×10^{-1}	97.8	n.a.	47.7	1.54	n.a.	n.a.	3.3×10^{10}
Kirkgecit	29.05.2013	3.7×10^{-2}	1.5×10^{-3}	2.6×10^{-7}	0.4	96.9	9.0×10^{-4}	3.7×10^{-1}	1.1	n.a.	24.8	0.18	1.2	294.6	1.2×10^{8}
Bardakcilar	29.05.2013	6.0×10^{-2}	1.5×10^{-3}	1.1×10^{-6}	1.6	93.8	2.2×10^{-3}	2.9×10^{-1}	3.0	n.a.	40.1	0.20	1.3	294.9	1.8×10^{8}
Yenice Hidirlar	29.05.2013	6.4×10^{-3}	1.4×10^{-3}	4.0×10^{-8}	0.4	93.6	6.0×10^{-4}	3.3×10^{-1}	4.1	n.a.	4.44	0.18	1.6	294.6	2.6×10^{9}
Yenice Hidirlar	03.09.2014	4.3×10^{-2}	3.9×10^{-3}	1.8×10^{-3}	0.3	97.8	1.2×10^{-4}	3.3×10^{-1}	1.5	n.a.	11.0	0.17	n.a.	n.a.	1.5×10^{8}
Uyusham. E-8	08.06.2013	1.3×10^{-3}	1.7×10^{-3}		0.7	4.7	3.0×10^{-5}	1.1×10^{-2}	94.2	n.a.	0.72	0.72	0.4	302.9	7.5×10^{10}
Uyushamam	08.06.2013	3.3×10^{-2}	1.4×10^{-3}		0.4	60.3	2.0×10^{-5}	3.6×10^{-2}	38.3	−2.5	23.6	0.66	0.9	299.2	1.2×10^{9}
Kuzuluk W	31.08.2014	1.8×10^{-2}	2.0×10^{-5}		0.3	4.4	9.0×10^{-5}	1.9	93.4	n.a.	897	0.65	n.a.	n.a.	5.8×10^{9}
Kuzuluk K-3	31.08.2014	6.7×10^{-3}	1.9×10^{-5}		0.1	2.4	3.0×10^{-5}	8.2×10^{-1}	96.7	n.a.	346	0.63	n.a.	n.a.	1.7×10^{10}
Armutlu kapl.	31.05.2013	6.4×10^{-4}	2.1×10^{-3}		0.0	37.7		1.3	61.0	−1.6	0.31	0.93	n.a.	n.a.	7.4×10^{10}
Armutlu IPA2	01.06.2013	1.0×10^{-1}	1.1×10^{-3}	2.5×10^{-8}		70.0	1.0×10^{-5}	5.3	23.7	−2.7	90.3	0.20	0.9	294.3	8.5×10^{8}
Armutlu well	01.06.2013	1.7×10^{-2}	1.6×10^{-3}		6.1	42.6	7.0×10^{-5}	1.3	49.3	−1.1	10.5	0.26	0.7	299.2	8.3×10^{9}
Termal Göz	05.06.2013	8.0×10^{-3}	4.4×10^{-4}		0.4	22.5		9.5×10^{-3}	76.6	−6.1	18.3	0.11	0.5	303.2	6.1×10^{10}

4.1. Water Chemistry

Water samples were collected over a wide range of geo-tectonic, hydrogeological settings and rocks having different origin and mineralogy (sedimentary to volcanic and metamorphic environments). Accordingly, waters display a large variety of physico-chemical features and geochemical compositions as a function of the different processes and mixing (e.g., with seawater) occurring along the hydrological paths, irrespective of their outlet temperature. The outlet temperatures range from 14.1 °C (a *Çesme* in Yayaköy-Terkirdağ) to 97 °C (a hot spring in Tuzla, Çanakkale). The Çanakkale area hosts the hottest water of the whole Marmara area marked also by the highest values of electrical conductivity (93 mS/cm in Tuzla and 31.5 mS/cm in Kestanbol; Table 1). pH values

fall mostly in the range of 6.05–6.96. Extreme values of 9.01 and 3.87 are recorded at an artesian well in Yeniköy (Kocaeli) and in a *Çesme* at Ekşidere (Balikehir), respectively. The thermal waters with the highest outlet temperature show also the largest content of Na, Ca and Cl. Contrastingly, the lowest Na contents are not related to low-temperature waters. Waters with outlet temperatures in the range of 40–59.7 °C from the areas of Yalova, Bolu, and Eskişehir display Na contents as low as 0.4–0.6 meq/L. The Piper diagram of Figure 3 provides general information on the water types vented around the Marmara Sea. Their spatial distribution of the water chemistry is shown as pie charts in the appendices (Figure A2).

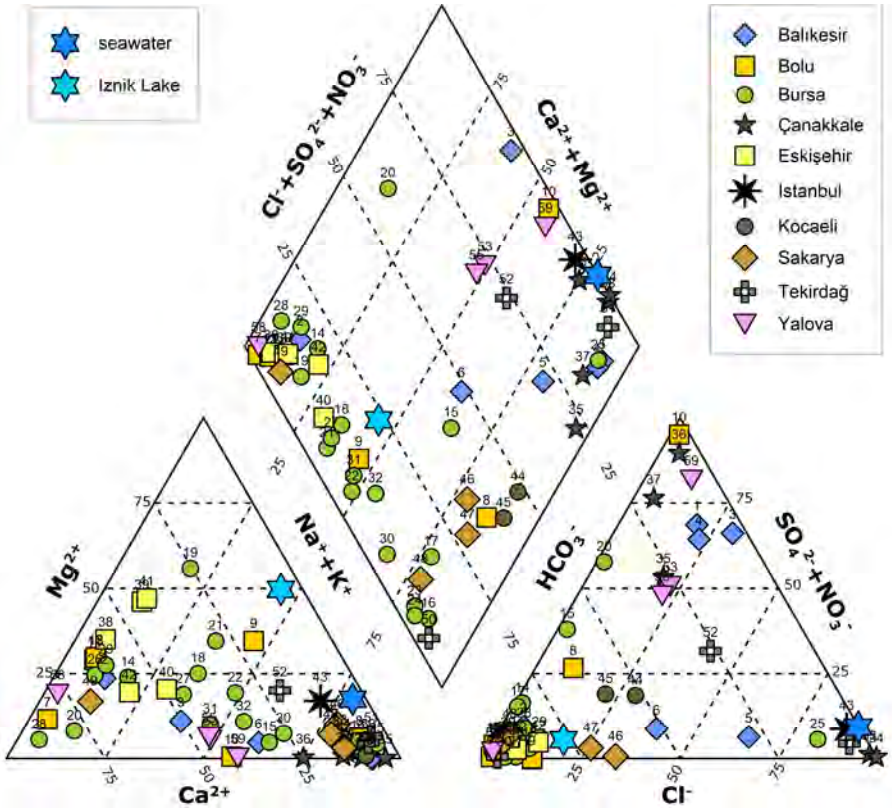

Figure 3. Piper diagram of the water samples as a function of the geographical areas. Sample labels as the ID numbers in Table 2.

The diagram shows how the thermal and mineral waters collected over the various areas surrounding the Sea of Marmara fall in the different water-type fields although samples collected over the same area (see samples from Bursa) fall in different fields as a consequence of the occurrence of mixing among different water types and WRI (water–rock interaction) processes due to different involved rock types and the extension of the processes.

4.2. Gas Geochemistry

4.2.1. Dissolved Gases

Table 3 lists the analytical results for the dissolved gases showing the presence of variable oxygen amounts and a total amount of gases dissolved in one liter of water which is usually 2–3 orders of magnitude higher than the equilibrium with the atmosphere (Air Saturated Waters, ASW = 16.8 cc/L_{H2O}). Only in a few cases is the total amount of dissolved gases significantly lower than the ASW (e.g., 7.8 cc in a sample from Termal, Yalova or 4.2 cc in samples from the Kocaeli area). The N_2/O_2 ratio, an indicator for atmospheric contamination, ranges between 2 and 7 (N_2/O_2 ratio in ASW = 2, Table 3) in the majority

of the collected samples, indicating negligible contents of atmospheric components. A few samples from Balikehir, Kocaeli, Çanakkale and Yalova are dominated by N_2. The most abundant gaseous component is CO_2 with concentrations well above the equilibrium with air-saturated water (ASW; 0.267 ml_{STP}/L_{H2O}, (Weiss, 1974) [48] ranging from 1 to 2 orders of magnitude above the equilibrium with the atmosphere. Over the area of Bursa (Table 3), we recorded the highest CO_2 contents with a pCO_2 of 0.88 bar at Çitli, Inegöl (ID = 24, Table 2) and of 0.82 bar at two wells in Kinik, Inegöl and Dümbüldek (ID = 23 and 30, respectively).

CH_4 is always present with concentrations ranging from 1.5×10^{-5} ml_{STP}/L_{H2O} at Tarakli (Sakarya, ID = 49, Table 3) thermal well to 5.49 ml_{STP}/L_{H2O} at Yayaköy (Tekirdag, ID = 51) mineral spring.

The isotopic composition of the Total Dissolved Carbon ($\delta^{13}C_{TDC}$) ranges between −17.47 ‰ and +2.9 ‰.

The concentrations of light noble gases (He, Ne and Ar) in the dissolved gases vary from 7.6×10^{-5} to 6.3×10^{-3} ml_{STP}/L_{H2O}, always above the equilibrium with ASW (4.8×10^{-5} ml_{STP}/L_{H2O}), with an isotopic signature ranging from 0.34 to 4.41 Ra (Ra = $^3He/^4He$ atmospheric ratio). The He/Ne ratios are always above 0.267, considered as the reference for an ASW by Holocher et al., 2002 [49].

4.2.2. Bubbling Gases

The bubbling gases are normally not air-contaminated, as shown by the low oxygen contents, except two samples from wells located in Mudurnu and Armutlu (see ID 12 and 56 in Table 4). CO_2 is the main gas for most of the collected samples with concentrations above 90 vol.%. Lower CO_2 contents (from 23.4 to 76.6 vol.%—see Table 4) are associated with a virtual increase in low-soluble gases (He, N_2, CH_4). CH_4 is present in a wide concentration range: from very low values (e.g., 0.003 vol.% in sample 7 from Çepni, Bolu) to >90 vol.% CH_4 from the site Çakırlı (ID = 27, Table 4) at Lake Iznik in the Bursa province. Helium is always enriched by 1 to 3 orders of magnitude with respect to the equilibrium with the atmosphere, both in bubbling and dissolved gases.

The $\delta^{13}C_{CO2}$ values are in the range of −17.23–1.1‰. The He content in the bubbling gases ranges from 1.5×10^{-5} to 5.9×10^{-2} vol.%; the He/Ne ratios vary from 0.31 (the same as atmospheric ratio) to 897 with isotopic helium signatures ranging from 0.18 to 1.60 Ra (uncorrected for atmospheric contamination).

5. Discussion

5.1. Water Geochemistry

Several geochemical "water types" Ca-HCO_3, Na-HCO_3, Ca-SO_4, Na-SO_4 and Na (Ca)-Cl (SO_4) were identified in the collected samples due to the geologic complexity of the Marmara area. Besides the chemistry, both thermal and mineral waters exhibit a large variability in the physico-chemical parameters (Table 2), driven by the occurrence of different geochemical processes (i.e., water–rock interaction, mixing between aquifers, dissolution of gases of different origins, repeated gas–water interactions, etc.) affecting the final water's features.

We found Ca-Mg-HCO_3 type in cold and warm waters circulating in the Bursa, Bolu and Eskişehir sectors where most of the samples are calcium-dominated. The molar ratios of calcium to magnesium ion concentration as well as calcium vs bicarbonate provide information on the rock type from which a spring is emerging (Figure 4). In waters discharging from carbonate rocks, dolomite dissolution brings the Ca/Mg ratio near unity, whereas a higher ratio (typically in the range of 6–8, White 2010 [50]) is indicative of larger calcite contribution.

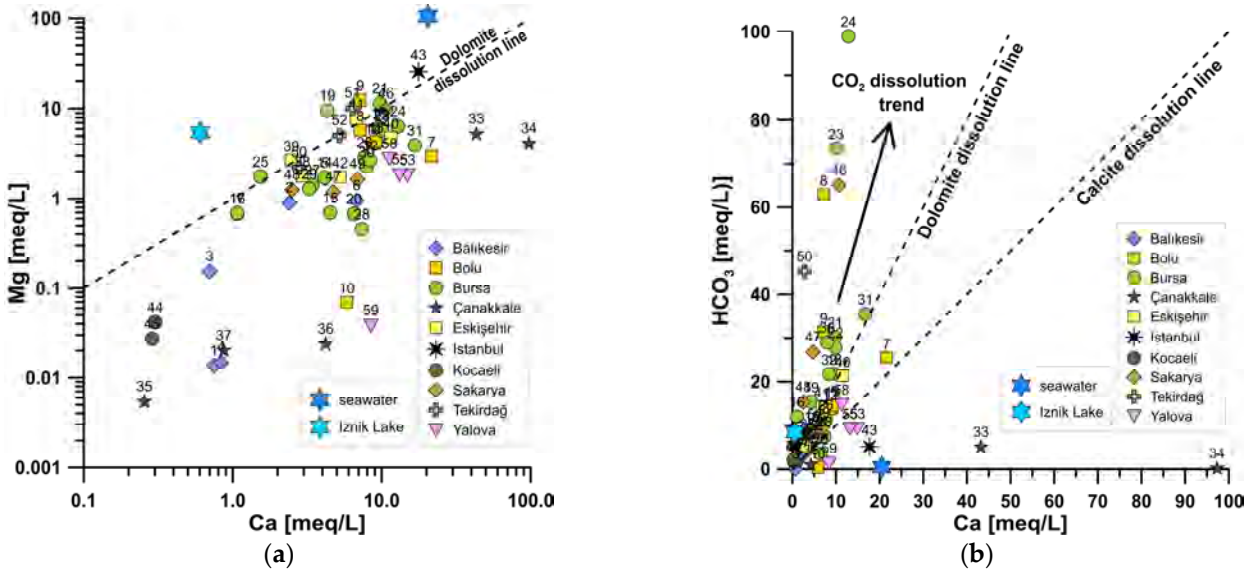

Figure 4. Ca vs Mg (**a**) and HCO_3 (**b**). The occurrence of GWI processes allows CO_2 dissolution that is responsible for the observed geochemical features related to WRI resulting in dolomite and calcite dissolution to various extents. Sample labels are the same as the ID numbers in Table 2.

Samples from deep wells in Bursa and from Kocaeli have high pH values (>8.0) and very low Ca and Mg contents (Tables 1 and 2), causing high alkali metal (mainly Na)/alkaline earth metal ratios. The chemical evolution of these waters could derive from a direct ionic exchange with clays: Ca^{2+} (Mg^{2+}) + Na-X → Ca (Mg)-X_2 + Na^+ (e.g., Giménez and Morell 1997 [51]).

Cold, warm and thermal Na-HCO_3-type waters mainly occur in the Bursa and Sakarya sectors (Figure 5a). Na-HCO_3 waters support a combination of WRI (Water–Rock Interaction) and GWI (Gas–Water Interaction) processes due to high CO_2 flux and extensive water–rock dissolution, together with ion exchange reactions in deep aquifers at high temperatures. The CO_2 can thus be considered as the trigger for the intensified water–rock interactions in a silicate environment and enhance leaching of dissolved ions in the thermal waters (e.g., White, 2005; Navarre-Sitchler and Thyne, 2007 [52,53]).

Na-Cl type waters (Figure 5b) include three thermal waters, one warm sample and four cold waters showing how they circulate both along the Marmara Sea (Istanbul, Tekirdag) and the Aegean Sea (Çanakkale) coastlines as well as in some inner sectors (Lake Iznik, Bursa, Balıkesir, Sakarya). It is generally accepted that Na/Cl > 1 may clearly indicate that the groundwater is far from seawater intrusion as seawater contribution brings a typical Na/Cl ratio around 0.8–0.9. Waters with significantly lower Cl concentrations and Na/Cl >> 1 can be interpreted as Na derived from water–rock interactions, usually released from a silicate weathering reaction of rock-forming minerals (Figure 5b). The molar ratio of Na/Cl for groundwater samples of the study area spans over a small range, from 0.80 to 1.40, very close to the local seawater ratio (0.86).

Thermal waters from Tuzla (Çanakkale) and Kestanbol can be defined as highly saline waters (Stanton et al. 2017 [54]) or classified as a brine (TDS > 35 g/L e.g., Rhoades et al., 1992 [55]). Balderer (1997) [56] and Mützenberg (1997) [44] suggested that the Tuzla brines derived from lateral migration of fossil brines trapped in Miocene sediments. For other Na-Cl-type waters located tens of kilometers away from the closest sea, mixing with deep-seated brines and/or fossil waters must be taken into account to justify their chemical features, as recognized elsewhere in Turkey (e.g., Mutlu & Gulec, 1998) [57].

The Na-SO_4 water type is generally associated with metamorphic/volcanic rocks coupled with H_2S condensing into the liquid phase as well as from interaction with sul-

phur/sulphate minerals (e.g., Ellis and Mahon, 1977 [58]). SO_4 enrichment (Figure 6) of the hot-water samples from Balıkesir and Çanakkale is not in stoichiometric equilibrium with Ca, suggesting that gypsum/anhydrite cannot be the main source of sulphate in Na-SO_4 waters. Na release into solution and calcium and magnesium removal could be the result of a direct ionic exchange with clays, as already inferred from some Na-HCO_3 waters.

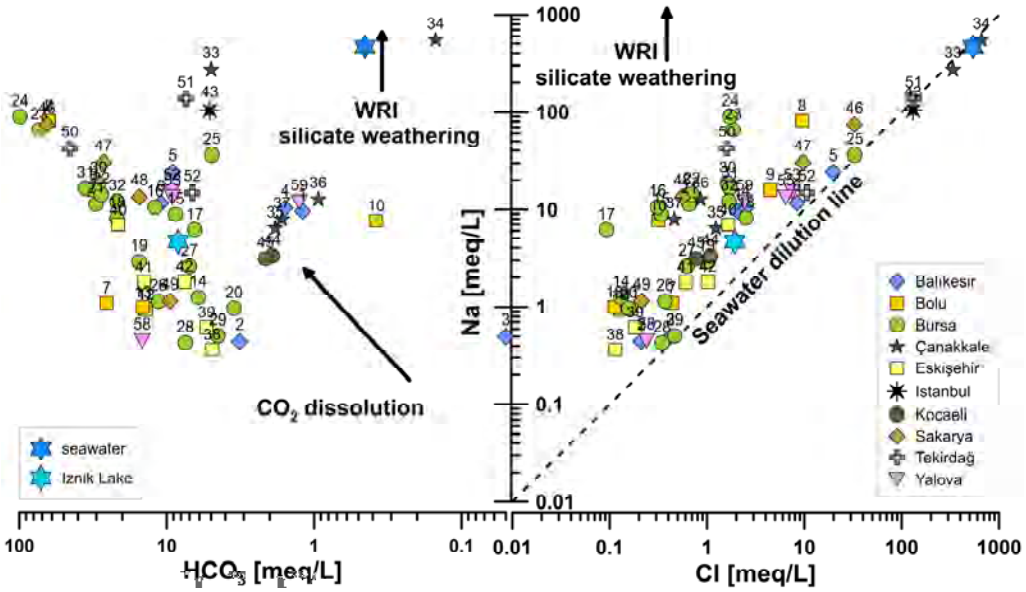

(**a**) (**b**)

Figure 5. Na vs HCO_3 (**a**) and Na vs. Cl (**b**). The occurrence of WRI and GWI processes is responsible for the observed geochemical features. Blue star symbol = sea water. Sample labels are the same as the ID numbers in Table 2. Symbol colors are as shown in Figure 3.

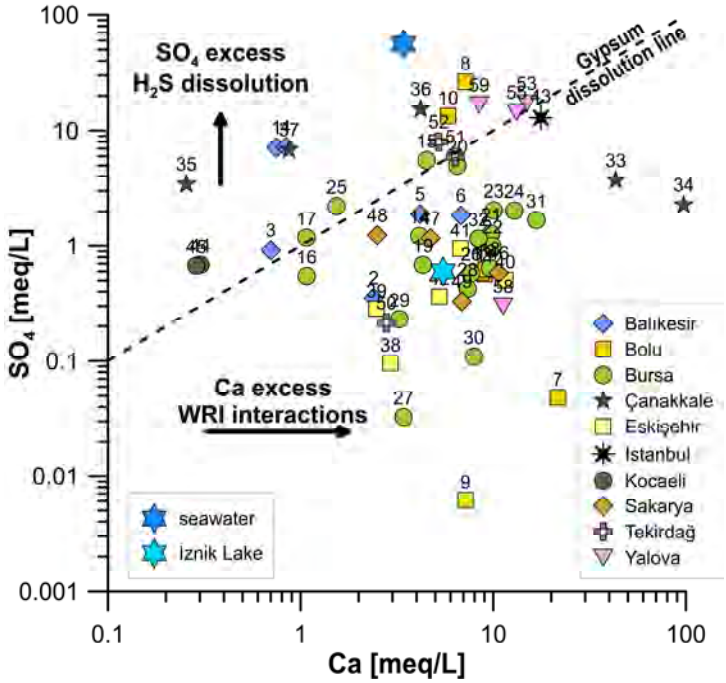

Figure 6. Ca-SO_4 plot showing that gypsum dissolution is not the main process responsible for the SO_4 ions, with the water chemistry being a consequence of WRI and GWI processes. Sample labels are the same as the ID numbers in Table 2. SW = sea water.

The acid-sulphate-type water was found just in one sample located in the Balıkesir province called Ekşidere "*Gencli Su*" (ID = 3). Low temperature and salinity along with the particularly acidic pH (3.87) of this shallow water suggest a probable oxidation of sulphide deposits near the spring. Indeed, sulphides are oxidized when exposed to the environment, due to natural processes or anthropogenic activities, forming sulfuric acid in the presence of humidity (Bigham and Nordstrom, 2000, and references therein) [59]. This process contributes to the acidification of natural waters.

5.2. Stable Isotopes

The measured $\delta^{18}O$–δD values are consistent with a meteoric origin of the groundwater. Figure 7 shows how most of the waters plot between the Global Meteoric Water Line (GMWL, Craig 1961) [60] and the Eastern Mediterranean Meteoric Water Line (EMWL, Gat and Carmi 1970) [61].

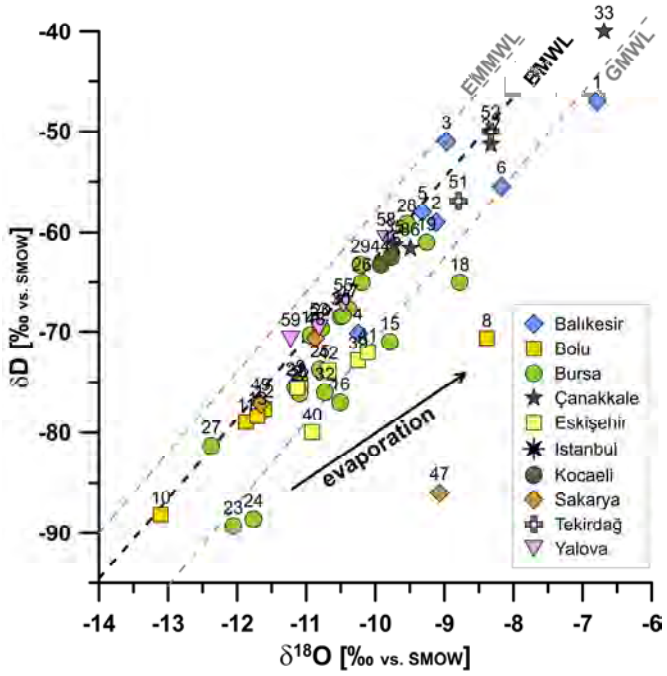

Figure 7. $\delta^{18}O$–δD plot for the collected waters. Samples fall between the two reference lines representing the EMMWL (Eastern Mediterranean Meteoric Water Line; Hatvani et al., 2023 [62]) and the GMWL (Global Meteoric Water Line; Rozanski et al., 1993 [63]). BMWL refers to the Bursa local meteoric water line proposed by Imbach et al. (1997) [38]. Sample labels are the same as the ID numbers in Table 2.

The large interval of the measured values, irrespective of outlet temperatures, can be explained considering the size of the studied region and the geographical differences among the sampling sites. A more detailed inspection of the plot of Figure 7 highlights that some mineralized hot, warm and cold waters (TDS in the range 1100–8500 mg/L) show slight to moderate positive shifts in $\delta^{18}O$ as in the case of samples 8, 46 and 47.

Their deviation from the MWLs can be attributed to water–rock interaction and/or phase separation processes including exchange between thermal fluids and oxygen-bearing minerals. High-temperature water–rock interaction processes can play an important role in changing not only the chemical (see Section 5.1) but also the isotopic composition of these waters. In particular, the sample from an abandoned well in Kuzuluk (Sakarya, ID = 46) plots off the water lines showing a remarkable $\delta^{18}O$ shift (nearly 12‰ V-SMOW), indicating that its isotopic composition is affected by intense evaporation, mixing with

evaporated water and/or phase separation; however, an extensive water–rock interaction process cannot be ruled out.

5.3. Gas Composition

The analytical results of the gas phase (Tables 3 and 4) indicate that the gases released around the Sea of Marmara are dominated either by N_2 or CO_2. The diagram N_2-CO_2 of Figure 8 clearly highlights how the bubbling gases are a binary mixture of two end members. The increase in N_2 content as CO_2 decreases shows that the chemical composition of the bubbling gases is the result of the combination of two effects: mixing between components of different origin and Gas–Water Interactions (GWIs) that lead to CO_2 loss due to dissolution and consequent virtual N_2 increase. The presence of a third component CH_4-dominated is shown in the analytical results (see Tables 3 and 4). The gas from a Çesme in Çakırlı, located at the northern shore of Lake Iznik (ID = 27 in Figure 8 falling outside the CO_2-N_2 mixing trend) is mainly composed of methane. See also Figure A3 in the appendices.

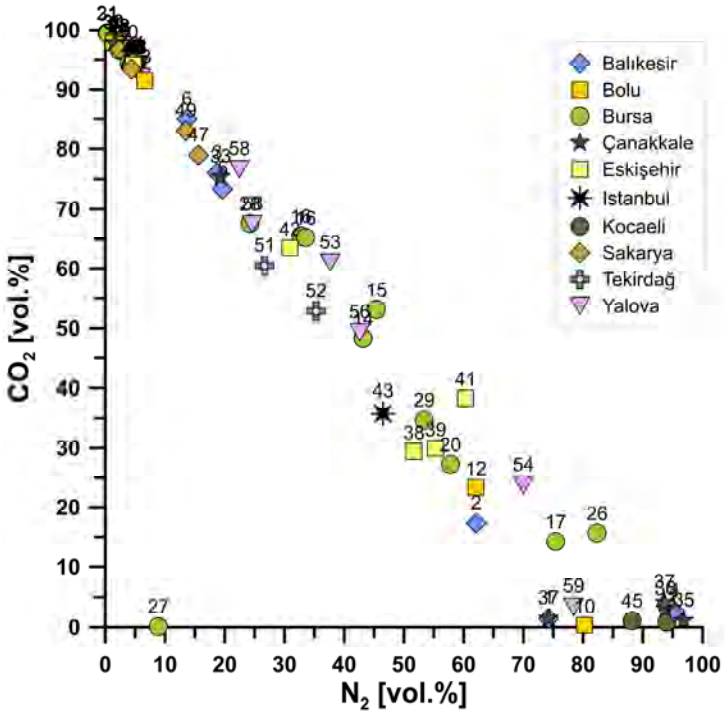

Figure 8. CO_2-N_2 relationships for bubbling (filled circles) and dissolved (diamond) gases indicating the presence of two end members in the gas phase, namely the shallow atmospheric-derived N_2 component and the deep-originated CO_2, vented over the Marmara area that mix at variable extents. Numbers indicate the sample IDs as in Table 1.

The CO_2-CH_4-N_2 triangular diagram of Figure 9 shows how the gases have CO_2 contents often above 90 vol.%, with the exception of the N_2-dominated gases from Çanakkale and the CH_4-dominated gas phase from some sites over the Yalova area. As the atmospheric component for the plotted samples has been removed assuming 0 oxygen content for the deep CO_2 and CH_4-dominated components, the nitrogen can have either a deep or an atmospheric origin from fluids where oxygen has been removed by bacterial or activity or oxidation processes.

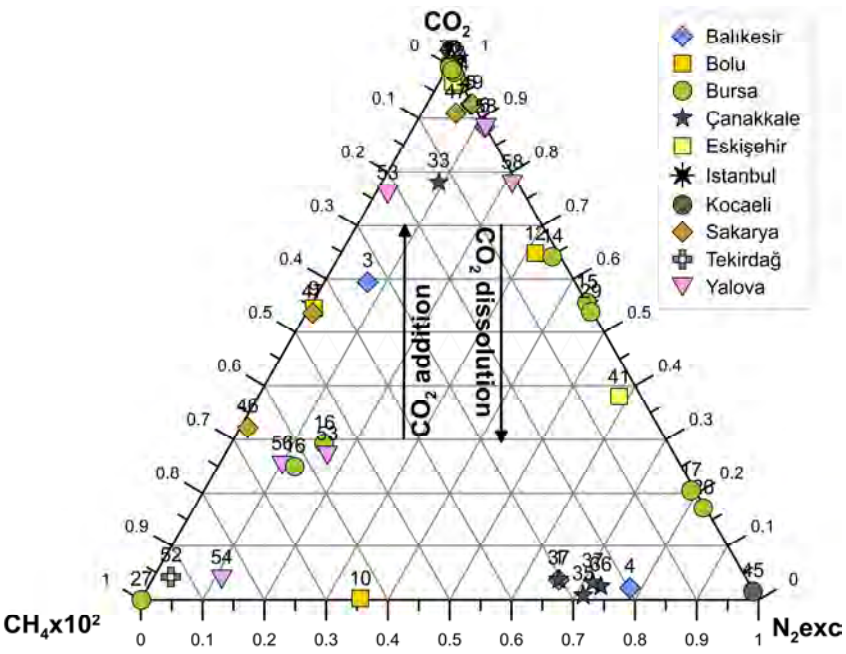

Figure 9. CO_2-CH_4-N_2 triangular diagram of the bubbling (filled circles) and dissolved (diamonds) gases showing the relative contents of the three end members N_2, CO_2 and CH_4. We plotted the N_2 excess with respect to the atmospheric nitrogen. The arrows highlight the GWI processes (CO_2 loss and increased N_2 and CH_4 contents) as well as mixings due to CO_2 addition from various sources that significantly changed the composition of the pristine gas phase. The numbers beside the symbols indicate the site as listed in Table 1.

5.4. Helium–Carbon Systematics

As CO_2 is the main component in most of the vented fluids, we argue that deep-originated gases feed most of the investigated manifestations. To trace their origin, we take into account that the natural CO_2 sources are marked by different $\delta^{13}C$ ratios ($\delta^{13}C_{MORB} = -6.5‰$; $\delta^{13}C_{Limestones} = 0‰$, $\delta^{13}C_{Marine\ sediments} = -20‰$ (Faure, 1986; Javoy et al., 1986; Sano and Marty, 1995) [64–66], although mixing of volatiles from different sources and fractionation processes may produce similar $\delta^{13}C$ values. The range of measured carbon isotopic compositions for Total Dissolved Inorganic Carbon (TDIC) ($-17.47‰ < \delta^{13}C_{TDIC} < +3.52‰$) and CO_2 ($-17.23‰ < \delta^{13}C_{CO2} < -1.1‰$) allows us to exclude a major role of organic CO_2 in the gas mixtures (typically ranging from $-70‰$ to $-25‰$; Figure 10). The trend shown in Figure 10a,b suggests that the vented CO_2 is not solely controlled by shallow interactions with groundwaters, and that the coexistence of multiple sources has to be considered.

The isotopically heavy carbon $\delta^{13}C_{TDIC}$ values (widespread in the Bursa waters and spotty in those circulating in the Çanakkale and BalıkesirBalikesir areas) suggest a contribution from carbonate devolatilization, likely sourced from high-temperature water–rock interactions. Although any high-temperature interaction requires a thermal source (e.g., the mantle and/or magmatic intrusions in the crust (Italiano et al., 2008) [67]), CO_2 from those sites (Bursa, Çanakkale and Balıkesir) is isotopically different from those of the Ganos/Tekirdağ area, which are depleted in heavy carbon ($\delta^{13}C < -17$ ‰), probably due to intense GWI.

The measured $^3He/^4He$ ratios span from 0.10 to 4.43 R/Rac, indicating a widespread mantle contribution at all sampled sites. Mantle helium does not show any obvious relation to the distribution of volcanic or intrusive igneous rocks (see Figure A4 in the Appendix C.3). It is frequently argued that extensional regimes enhance the helium escape through the crust. If that is true, the southwestern segment of our investigated area would be the most

promising—but not confirmed by data. The highest Ra was found at the eastern end of the Ganos fault (ID = 50 in Figure 2). The highest mantle helium contributions (up to 70%, R/Rac 4.3–4.6) were found offshore at a site called "Boris Bubblers", which is located some kilometers NE of the shoreline where the Ganos fault enters the Sea of Marmara (Burnard et al., 2012) [68]. The authors ruled out present-day magmatic activity and concluded that the release of mantle helium is related to the tectonic setting either coming directly from the mantle via high-permeability faults or else that He stems from cooling magma batches intruded in the shallow crust.

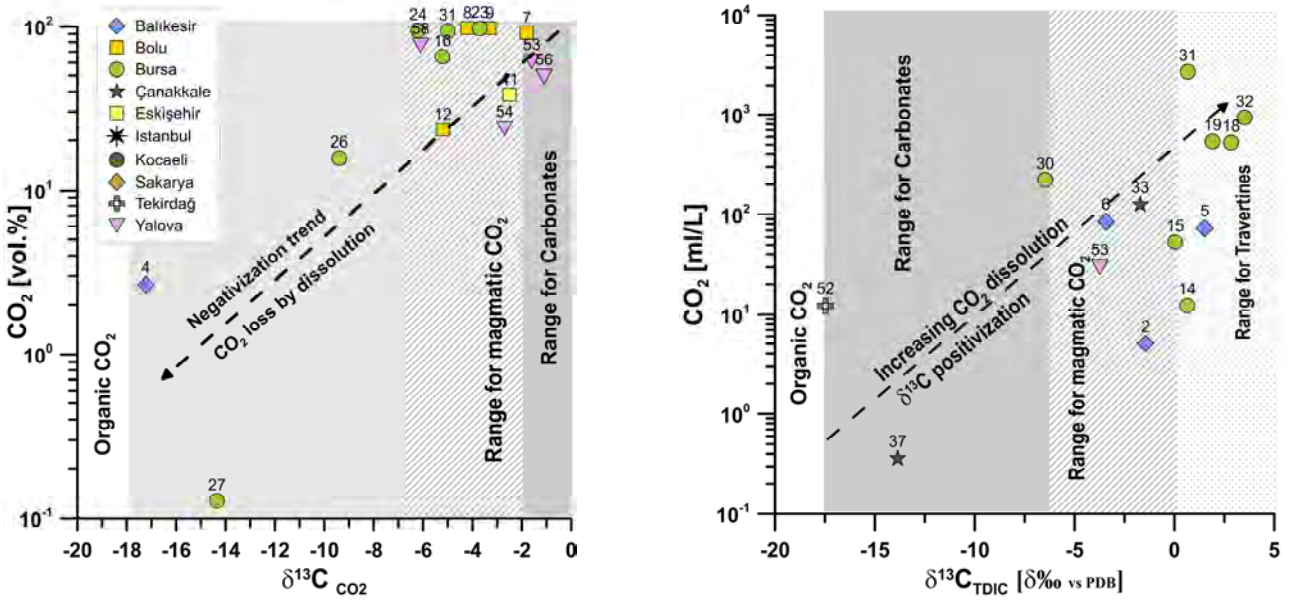

Figure 10. CO_2 content vs $\delta^{13}C_{CO2}$ for the bubbling gases (**a**) and for $\delta^{13}C_{TDIC}$ of the dissolved gases (**b**). The plots depict a clear direct correlation between isotopic ratios and CO_2 and HCO_3 contents. The contemporary trends denote the fractionation with quantitative loss of gaseous CO_2 and its heavy isotope as well as the occurrence of further fractionation processes. The occurrence of similar trends followed by samples from different sites around the Marmara area suggests that the vented CO_2 is not solely controlled by shallow interactions with groundwaters, and that the coexistence of multiple sources has to be considered.

The helium vs. $^4He/^{20}Ne$ isotopic ratios for both dissolved and bubbling gases are shown in Figure 11. Assuming all neon of atmospheric origin, the $^4He/^{20}Ne$ ratio provides an indication of the presence of an atmospheric-derived component in the gas mixture. The plot shows that the dissolved gases (diamonds in the picture) display $^4He/^{20}Ne$ ratios remarkably higher than the ASW although extracted from groundwaters equilibrated with the atmosphere as a consequence of a significant contribution of He-rich gases coming from the CO_2-dominated end member.

Helium–carbon relationships in terms of both elemental and isotopic ratios (Figure 12) show the wide range of $CO_2/^3He$ ratios due to both elemental fractionation (GWI) and mixing between crustal and magmatic sources. Although some of the vented volatiles are highly fractionated, the widespread contribution of a mantle component is evident. The arrows in Figure 12 display the combined effect of regional degassing of magmatic and crustal components (represented by ^4He and ^3He, respectively) with the GWI inducing CO_2 loss for bubbling gases and addition for the ASW-type waters.

Overall, our results indicate that the fluids circulating over the Marmara area are the result of mixing at variable extents of three end members: mantle, crust and atmosphere.

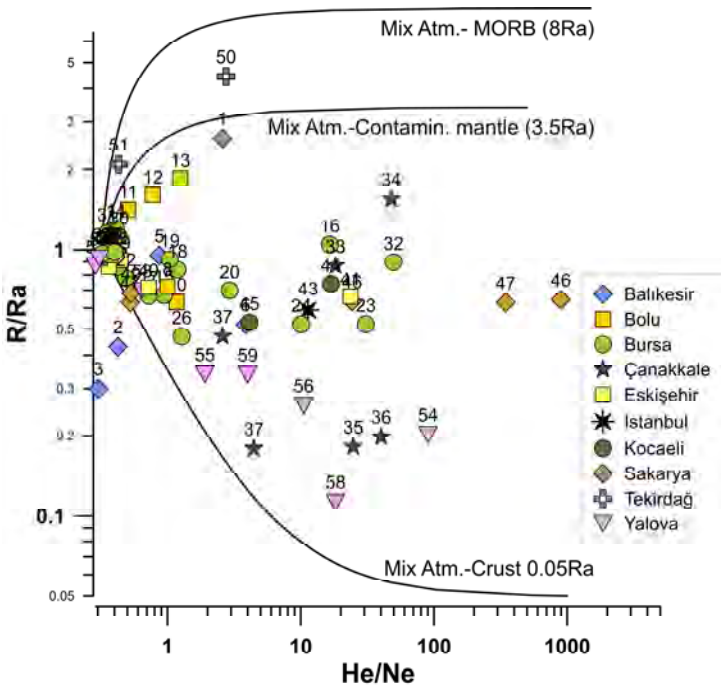

Figure 11. Helium isotopic ratios (uncorrected R/Ra values) and $^{4}He/^{20}Ne$ relationships for both dissolved and bubbling gases. The theoretical lines represent binary mixing trends of atmospheric helium with mantle-originated and crustal helium. The assumed end members for He-isotopic ratios and $^{4}He/^{20}Ne$ ratios are ASW (1 Ra, He/Ne = 0.267: Holocer et al., 2002) [49]; 8Ra for a MORB-type mantle; and 3.5 Ra for contaminated mantle; crust 0.05Ra and $^{4}He/^{20}Ne$ ratio = 10,000. Filled circles = bubbling gases; filled diamonds = dissolved gases. Sample IDs are as reported in Table 3. All error bars are within the symbol size.

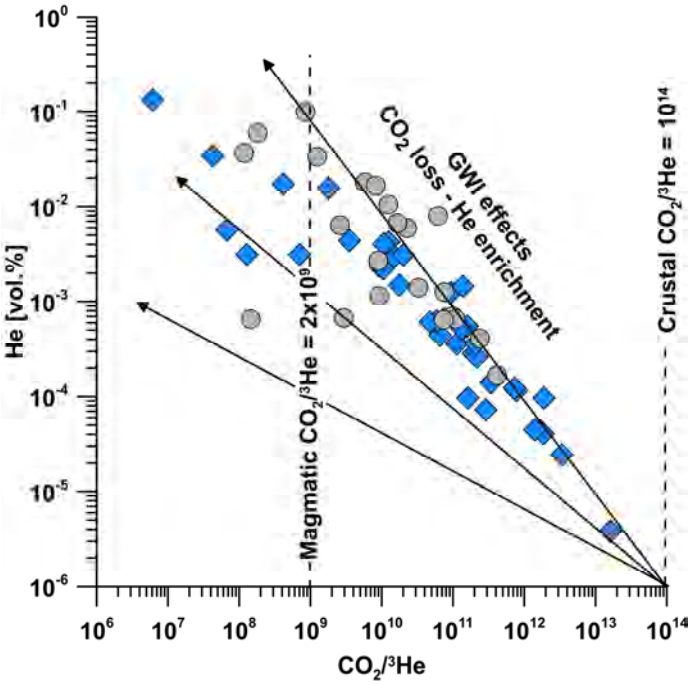

Figure 12. $CO_2/^{3}He$–^{4}He. The plot shows how the vented gases are a mixture of two main components: magmatic-type and crustal-originated. Circles = bubbling gases; diamonds = dissolved gases. The arrows display the main trends affecting the composition of the gas phase.

5.5. Fluid Circulation and Fault Activity

While the composition of crustal fluids circulating at relatively shallow depths (namely 3–5 km) is determined by the local geology (for example, the hosting rocks where thermal waters equilibrate or where ground waters interact with gases), the composition of deep fluids is closely influenced by tectonics. Actually, since mantle degassing is not obvious in non-volcanic areas, we argue that if the recorded helium isotopic ratios are higher than the typical crustal values, the release of ^{3}He through lithospheric faults is one of the possibilities. Additionally, as intense mantle degassing along faults cutting 15–25 km of crustal thickness cannot be supported by very low vertical permeability (Italiano et al., 2000) [69], mantle-derived volatiles may be related to melts intruded in crustal levels as already observed in Southern Apennines by Italiano et al., 2000 [69]. Alternatively, the ductile to fragile transition layers for the various NAFZ segments occur at shallower levels than 15–25 km.

Evidence that fluids with a variable—although sometimes significant—mantle component are vented over the whole Marmara region implies a widespread lithospheric character of the various NAFZ branches, highlighting the possibility of detecting variations in the fault behavior from temporal and spatial changes in the mixing proportion of the deep and shallow fluid components. Unfortunately, repeated measurements of helium isotopes are rare as the compilation of published data shows (see Appendix C).

In the past, the most significant decrease in the mantle helium contribution was observed at Mudurnu and Efteni (ID = 11 and 9), both located in the easternmost segment in the province of Bolu. In 1995, i.e., before the Izmit and Düzce earthquakes of 1999, Ra values of 4.65 and 1.83 were observed at Mudurnu and Efteni, respectively. In 2000 and the following years, the Ra values decreased to 2.19 and 0.81, respectively (see Table A1 in the appendices). Dogan et al. (2009) [46] assumed that the decrease in mantle helium at Mudurnu might be related to a large post-seismic increase in water level. Mudurnu is a free-flowing artesian well and we can confirm from our own observations that the water flow almost doubled after the 1999 earthquakes. Interestingly, the physico-chemical parameters were not affected by the earthquakes (Woith et al., 2000) [70]. For Efteni, the authors state that the reduced mantle helium was probably caused by a decreased permeability of the faults. Again, we confirm from our own observations that the water stopped flowing immediately after the Düzce earthquake of 13 November 1999. Two weeks after the event, the flow rate recovered to pre-event levels and we could take a water sample. The chemical composition did not change, but we measured a 4-fold increase in dissolved CO_2 (Woith et al., 2000) [70].

6. Conclusions

The MARsite project enabled us to collect enough data (59 sites) for the evaluation of the background geochemical features of fluids venting over the study area. All the collected information indicates that the fluids circulating over the Marmara Sea area are the result of mixing of three gaseous end members (mantle, crust and atmosphere) at variable extents. Thermal and mineral waters equilibrated at various depths in a wide range of hosting rocks.

- Water geochemistry: Water temperatures range from 14 °C to 97 °C, and electrical conductivity from 198 µS/cm to 93 mS/cm. Geochemical "water types" Ca-HCO_3, Na-HCO_3, Ca-SO_4, Na-SO_4 and Na (Ca)-Cl (SO_4) indicate the geologic complexity of the Marmara area driven by the occurrence of different geochemical processes (i.e., water–rock interaction, mixing between aquifers, dissolution of gases of different origins, repeated gas–water interactions, etc.) affecting the final water's features.

- Stable isotopes: The measured $\delta^{18}O$–δD values are consistent with a meteoric origin of the groundwater and denote the occurrence, sometimes significant, of evaporation effects.
- Gas composition: Bubbling gases are a binary mixture of two end members, namely CO_2 and N_2. Only a few samples contain CH_4 in significant amounts. The increase in N_2 and CO_2 decreases shows that the chemical composition of the bubbling gases is the result of the combination of two effects: mixing between components of different origin and Gas–Water Interactions (GWIs) that lead to CO_2 loss due to dissolution and consequent virtual N_2 increase.
- Helium–carbon systematics: The measured $^3He/^4He$ ratios span from 0.11 to 4.43 R/Ra, indicating a widespread mantle contribution at all sampled sites. Mantle helium does not show any obvious relation to the distribution of volcanic rocks. Spatial variations of the $^3He/^4He$ isotopic ratios are possibly related to fault segments with different rock permeability. High isotopic ratios do not exclude the presence of magmatic intrusions in the shallow crustal levels.

The geochemical features of the fluids, including cold and hot waters and the dissolved and bubbling gases vented along the NAF segments around the Sea of Marmara, are the consequence of interactions between a deep (mantle-derived) component that mixes at variable extents with groundwater circulating at variable levels in the shallow crust. Changes in geochemical parameters have been reported in coincidence with seismic events and we argue that they should be expected during the entire seismogenic cycle, even in the absence of seismic energy release (e.g., Italiano et al., 2009 [71], Wang and Manga, M., 2015 [72], Sato et al. 2020 [73] and references therein).

Since changes in vertical permeability and microfracturing induced by stress accumulation and crustal deformation play a significant role in the fluid circulation, they are responsible for temporal changes observable in the fluids' geochemistry. This close relationship between fluid geochemistry, stress accumulation and fault behavior represents the scientific reference for the development of a multidisciplinary monitoring activity over the Marmara region, where fault failures are expected. Our results can be the reference for future periodical geochemical surveys and for the selection of the most suitable sites to set up automatic stations for continuous monitoring activity.

Author Contributions: F.I. and H.W. developed the conception and design of the study. F.I., H.W. and C.S. collected fluid samples during 2014. Analytical job carried out at INGV where L.P. and A.S. worked on the water analyses. F.I. wrote the first draft of the manuscript. C.S. drafted the original version of the database and worked on data validation. F.I. and H.W. took care of funding acquisition and project administration. All authors have read and agreed to the published version of the manuscript.

Funding: This research has received funding from the European Union's Seventh Programme for research, technological development and demonstration under grant agreement N° [308417] (MARsite project) co-funded by the European Commission THEME [ENV.2012.6.4-2].

Data Availability Statement: Data are available at http://dataservices.gfz-potsdam.de/portal/ (accessed on 1 February 2025).

Acknowledgments: The paper is a scientific contribution to the MARsite project. Field work and fluid monitoring were supported by TÜBITAK Marmara Research Centre, Earth and Marine Science Institute (Gebze, Turkey), Department of Geophysics, Kocaeli University (Kocaeli, Turkey), and GFZ German Research Centre for Geosciences (Potsdam, Germany). Comments and suggestions from two anonymous reviewers improved the earlier version of the manuscript.

Conflicts of Interest: The authors declare no conflicts of interest. The funders had no role in the design of the study; in the collection, analyses, or interpretation of data; in the writing of the manuscript; or in the decision to publish the results.

Appendix A

Locations

Location names are shown in Figure A1. Note that there are two sites called "Tuzla" in the investigation area (site ID = 34 south of Çanakkale and 43 east of Istanbul). Throughout the text "Tuzla" refers to site ID = 34.

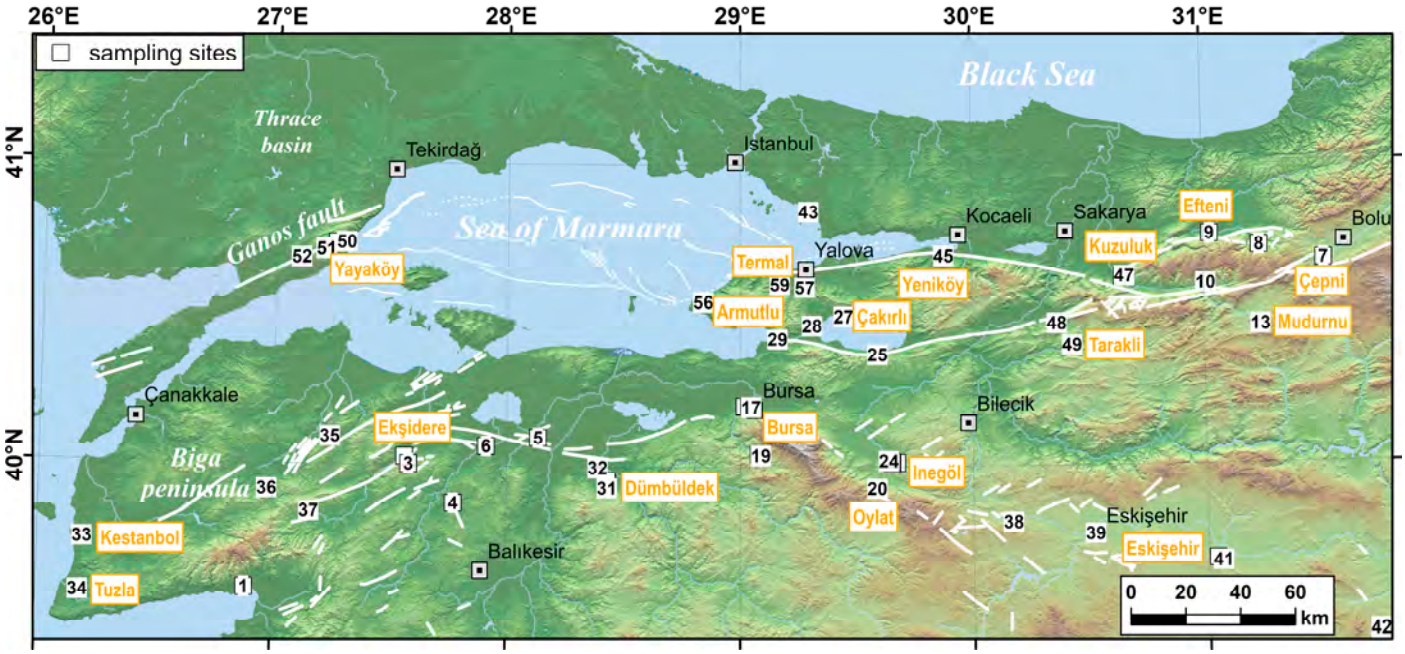

Figure A1. Map showing locations mentioned in the text. Numbers refer to sampling sites of this study (see Table 1).

Appendix B

Appendix B.1. Water Analyses

The concentration of the major ions was determined by liquid chromatography (Dionex 2001) using a Dionex CS-12 and a Dionex AS4A-SC column for cation and anion determinations, respectively. Water isotopic composition in terms of $\delta^{18}O$ and δD was determined by mass spectrometry by equilibration technique (Epstein and Mayeda, 1953 [74] for oxygen) and water reduction (hydrogen production by using granular Zn, Kendall and Coplen, 1985) [75], respectively, according to the procedure described in Yuce et al. (2014) [76] on unfiltered samples.

Measurements were carried out using a Finnigan Delta Plus mass spectrometer (Hydrogen) and an automatic preparation system coupled with an AP 2003 IRMS (Oxygen). The O and H isotopic data are expressed as per mil deviation from the V-SMOW standard (Vienna Standard Mean Oceanic Water) using the conventional $\delta^{18}O$ and δD notation ($\delta = [(R_{sample}/R_{standard}) - 1] \times 1000$ (‰) where R represents the $^{18}O/^{16}O$ or $^{2}H/^{1}H$ isotopic ratio). Analytical precision for each measurement is better than 0.2‰ for $\delta^{18}O$ and 1‰ for δD.

The partial pressure pCO_2 was computed by using the PHREEQC code v. 2.12 (Parkhurst and Appelo, 1999) [77], operating with the Lawrence Livermore National Laboratory (LLNL) database, having as input temperature, pH, Eh, alkalinity and major elements.

Appendix B.2. Gas Analyses

The chemical composition and the isotopic ratios of He and C of the bubbling and dissolved gases were determined using the same analytical equipment. The dissolved gases were extracted after equilibrium was reached at constant temperature with a host gas (high-purity argon) injected in the sample bottle through the rubber septum (details in Italiano et al., 2009, 2014 [78,79]). Chemical analyses were carried out by gas chromatography (Perkin Elmer Clarus500 equipped with a double TCD-FID detector) using argon as the carrier gas. Typical uncertainties are within ± 5%. The composition of the dissolved gas phase was calculated from the gas chromatographic analyses by combining the solubility coefficients (Bunsen coefficient in ml_{gas}/L_{H2O}) of each gas species at the equilibration temperature of the thermostatic bath, the extracted gas (ml) and the water sample volumes (carefully measured at the equilibration temperature) as in equation (A1):

$$GC = ([G_{gc}] \times * V\gamma_e + ([G_{gc}] \times ß_G \times V_W))/V_W \times V\gamma_e/V\gamma_i/100 \quad (A1)$$

where GC is the concentration of the selected gas, G_{gc} is its concentration measured by gas chromatography (vol%), $V\gamma_e$ and $V\gamma_i$ represent the extracted and the introduced gas volumes, respectively, $ß_G$ is the Bunsen coefficient of the selected gas species and V_W is the volume of the collected water sample.

Helium isotope analyses were performed on gas fractions extracted following the same procedure as for the gas chromatography, and purified following methods described in the literature (Sano and Wakita, 1988; Hilton, 1996; Italiano et al., 2001) [80–82]. After cryogenic separation of He from Ne, the purified helium fraction (either of dissolved or bubbling gases) was analyzed with a static vacuum mass spectrometer (GVI5400TFT) that allows the simultaneous detection of ^{3}He and ^{4}He ion beams, thereby keeping the ^{3}He/^{4}He error of measurement to very low values. Typical uncertainties in the range of low ^{3}He samples are within ±1%. During the same analytical procedure the ^{4}He/^{20}Ne ratio was measured by peak intensities on the mass spectrometer.

The carbon isotopic composition of CO_2 and CH_4 in bubbling gases was determined by a continuous flow mass spectrometer (Finnigan MATDeltaS). The sealed water samples were used for the carbon isotopic composition of total dissolved carbon ($\delta^{13}C_{TDC}$). It was measured in a 2 ml water sample introduced into containers injected with high purity helium to remove atmospheric CO_2. The water samples were acidified with phosphorus pentoxide in an auto-sampler to ensure complete release of CO_2 from acidified waters. CO_2 was then directly admitted to a continuous flow mass spectrometer (AP2003). All the results are reported in δ‰ units relative to the V-PDB (Vienna-Pee Dee Belemnite) standard; the standard deviation of the ^{13}C/^{12}C ratio was ± 0.2 ‰.

Argon isotopes were measured only in bubbling gases with a multi-collector noble gas mass spectrometer (ARGUS, GVI) specifically designed for simultaneous collection of ^{40}Ar, ^{38}Ar and ^{36}Ar isotopes on five Faraday collectors. ^{40}Ar is detected on a collector with a 10^{11} ohm resistor and the remaining isotopes are collected and measured on four detectors fitted with 10^{12} ohm resistors (for ^{36}Ar to ^{39}Ar). The equipment is connected to a stain-less steel purification line where 0.1 mL of gas are introduced and purified by cold and hot getter pumps (reactive gas removal). Measuring errors are estimated to be better than ±1%.

Appendix C

Appendix C.1. Water Chemistry

Figure A2 shows the chemical composition of the thermal and mineral waters around the Sea of Marmara.

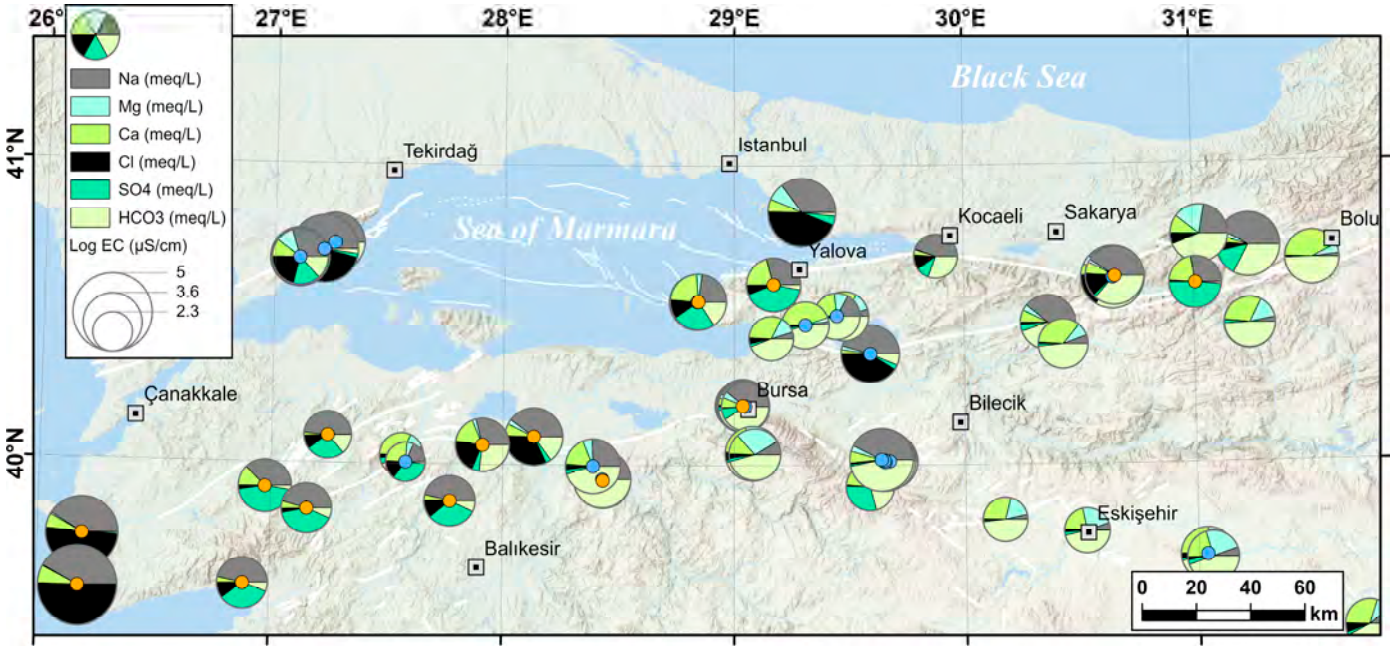

Figure A2. Chemical composition of thermal and mineral waters around the Sea of Marmara. The diameter of the pies scales with the specific electrical conductivity of the waters. Small circles in the centre of the pies indicate the water temperature: blue—cold (<20 °C); orange—hot (>40 °C).

Appendix C.2. Gas Composition

Figure A3 shows the gas composition in the investigation area.

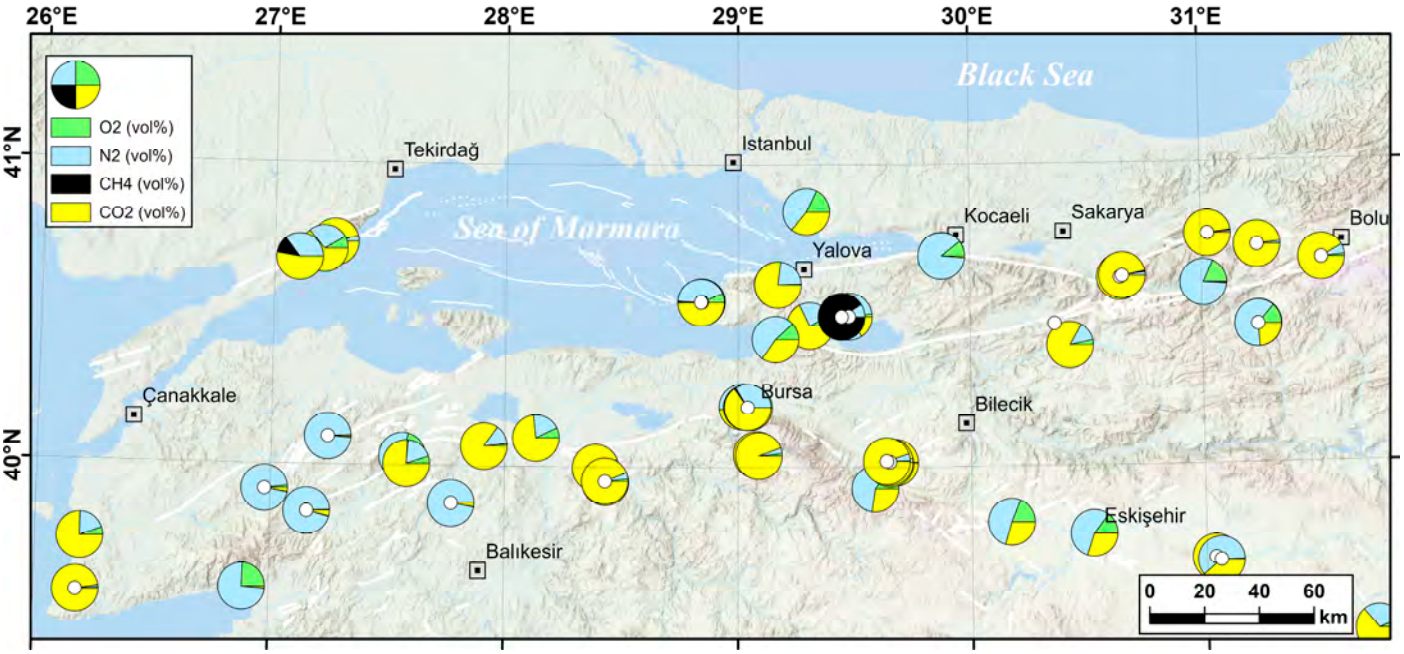

Figure A3. Gas composition of thermal and mineral waters around the Sea of Marmara. Small white circles in the centre of the pies indicate bubbling gases.

Appendix C.3. Helium Isotopes

The spatial helium R/Ra distribution is shown in Figure A4.

Table A1 lists a compilation of helium isotope values for the wider Marmara Sea area.

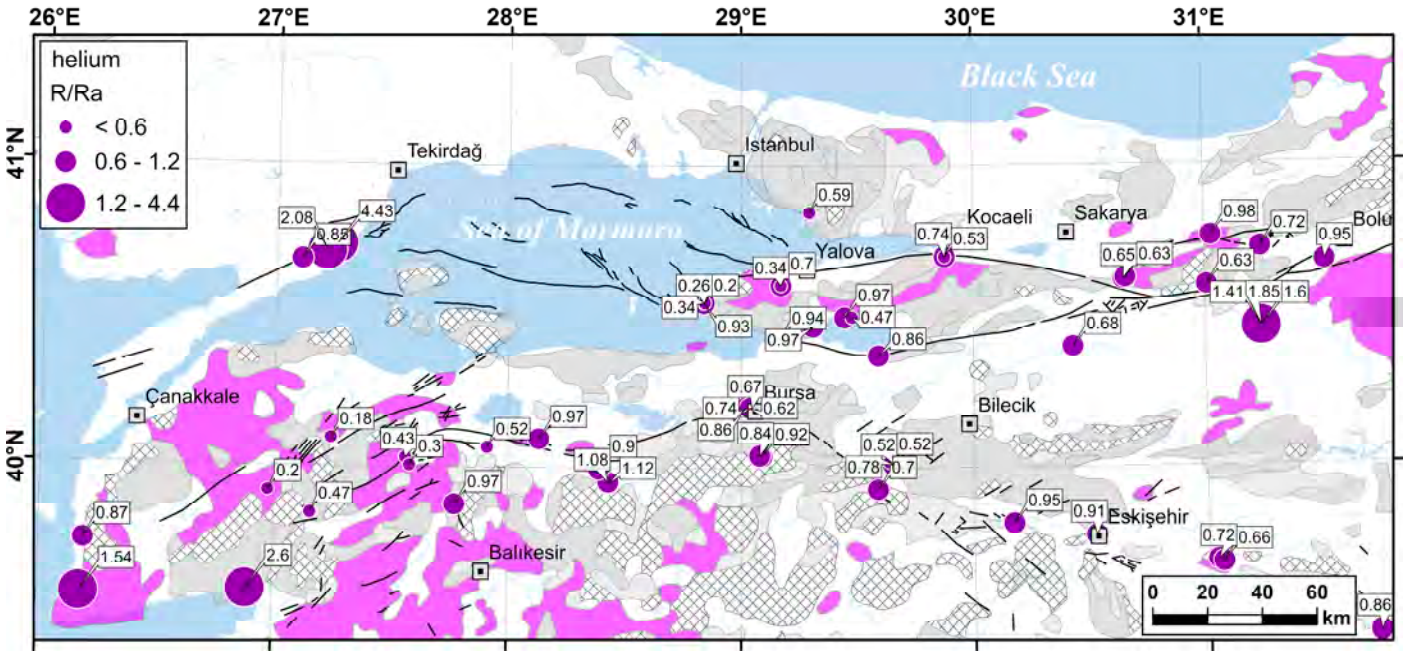

Figure A4. Helium isotope ratios given in R/Ra at mineral and thermal waters around the Sea of Marmara. Light purple areas depict Tertiary volcanic rocks, hatched areas mark intrusive igneous rocks of Paleozoic to Cenozoic age. Light and dark gray areas indicate Mesozoic and Paleozoic rocks, respectively. White areas are Paleogene to Quaternary sediments. Simplified geology modified from Pawlewicz et al. (1997) [83].

Table A1. Temporal evolution of helium R/Ra values between 1984 and 2014 compiled from various sources [44,46,84–92]. Data for 2013 and 2014 are from this study.

Site	ID	1984	1985	1989	1990	1992	1993	1995 [g]	2000	2001 [i]	2002 [i]	2003 [i]	2004 [i]	2005 [j]	2013	2014
Manyas Kizik	6													0.41 [k]	0.49	
Derdin	8	0.75 [a]						0.75						0.61	0.59	
Efteni	9	1.93 [a]						1.83	0.71 [h] 0.81 [i]	0.76	0.76	0.88	0.83	0.66		
Mudurnu	11	4.78 [a]						4.65	2.19 [h,i]		2.30	2.22	2.18	2.81	2.09	
Bursa Çekirge	14	0.52 [b]	0.60 [b]		0.48 [d]									0.48		0.46
Bursa Kükürt	15			0.44 [c]	0.45 [d]										0.54	0.46
Oylat	20													0.66	0.67	
Keramet	26	0.26 [a]						0.29						0.34	0.29	
Gemlik	29	0.05 [b]				0.15 [f]								0.13		
Kestanbol	33													0.80 [k]		0.87
Tuzla	34	0.42 [a]			1.47 [e]									1.44 [k]		1.55
Tuzla Büyüyk Iç.	43							0.42						0.52		0.58
Kuzuluk	47			0.63 [d]										0.63		0.63
Sarköy	50													4.85		4.80
Armutlu	53	0.22 [a]				0.24 [f]		0.41						0.25	0.22	
Yalova Termal	59					0.27 [f]			0.29 [h,i]		0.29	0.28	0.32	0.28	0.29	

[a]—Stone (1986); [b]—Gülec (1988); [c]—Imbach (1992); [d]—Greber (1992); [e]—Mützenberg (1997); [f]—Eisenlohr (1995); [g]—Ercan (1995); [h]—Gülec (2002); [i]—deLeeuw (2010); [j]—Dogan (2009); [k]—Mutlu (2008).

References

1. Wang, C.-Y.; Manga, M. *Earthquakes and Water*; Lecture Notes in Earth Sciences; Springer: Berlin/Heidelberg, Germany, 2010; Volume 114.
2. Mogi, K.; Mochizuki, H.; Kurokawa, Y. Temperature Changes in an Artesian Spring at Usami in the Izu Peninsula (Japan) and Their Relation to Earthquakes. *Tectonophysics* **1989**, *159*, 95–108. [CrossRef]

3. Malakootian, M.; Nouri, J. Chemical Variations of Ground Water Affected by the Earthquake in Bam Region. *Int. J. Environ. Res.* **2010**, *4*, 443–454.
4. Woith, H.; Wang, R.; Milkereit, C.; Zschau, J.; Maiwald, U.; Pekdeger, A. Heterogeneous Response of Hydrogeological Systems to the Izmit and Duzce (Turkey) Earthquakes of 1999. *Hydrogeol. J.* **2003**, *11*, 113–121. [CrossRef]
5. Heinicke, J.; Braun, T.; Burgassi, P.; Italiano, F.; Martinelli, G. Gas Flow Anomalies in Seismogenic Zones in the Upper Tiber Valley, Central Italy. *Geophys. J. Int.* **2006**, *167*, 794–806. [CrossRef]
6. Hilton, D.R. The Leaking Mantle. *Science* **2007**, *318*, 1389–1390. [CrossRef]
7. Mutlu, H.; Güleç, N.; Hilton, D.R.; Aydın, H.; Halldórsson, S.A. Spatial Variations in Gas and Stable Isotope Compositions of Thermal Fluids around Lake Van: Implications for Crust–Mantle Dynamics in Eastern Turkey. *Chem. Geol.* **2012**, *300*, 165–176. [CrossRef]
8. Woith, H.; Wang, R.; Maiwald, U.; Pekdeger, A.; Zschau, J. On the Origin of Geochemical Anomalies in Groundwaters Induced by the Adana 1998 Earthquake. *Chem. Geol.* **2013**, *339*, 177–186. [CrossRef]
9. Bozkurt, E. Neotectonics of Turkey—A Synthesis. *Geodin. Acta* **2001**, *14*, 3–30. [CrossRef]
10. Şengör, A.M.C.; Tuysuz, O.; Imren, C.; Sakinc, M.; Eyidogan, H.; Gorur, G.; Le Pichon, X.; Rangin, C. The North Anatolian Fault: A New Look. *Annu. Rev. Earth Planet. Sci.* **2005**, *33*, 37–112. [CrossRef]
11. Reilinger, R.; McClusky, S.; Vernant, P.; Lawrence, S.; Ergintav, S.; Cakmak, R.; Ozener, H.; Kadirov, F.; Guliev, I.; Stepanyan, R.; et al. GPS Constraints on Continental Deformation in the Africa-Arabia-Eurasia Continental Collision Zone and Implications for the Dynamics of Plate Interactions. *J. Geophys. Res.* **2006**, *111*, 26. [CrossRef]
12. Tatar, O.; Poyraz, F.; Gürsoy, H.; Cakir, Z.; Ergintav, S.; Akpınar, Z.; Koçbulut, F.; Sezen, F.; Türk, T.; Hastaoğlu, K.Ö.; et al. Crustal Deformation and Kinematics of the Eastern Part of the North Anatolian Fault Zone (Turkey) from GPS Measurements. *Tectonophysics* **2012**, *518–521*, 55–62. [CrossRef]
13. Duman, T.Y.; Çan, T.; Emre, Ö.; Kadirioğlu, F.T.; Baştürk, N.B.; Kılıç, T.; Arslan, S.; Özalp, S.; Kartal, R.F.; Kalafat, D.; et al. Seismotectonic Database of Turkey. *Bull. Earthq. Eng.* **2016**, *16*, 3277–3316. [CrossRef]
14. Armijo, R.; Meyer, B.; Navarro, S.; King, G.; Barka, A. Asymmetric Slip Partitioning in the Sea of Marmara Pull-Apart: A Clue to Propagation Processes of the North Anatolian Fault? *Terra Nova* **2002**, *14*, 80–86. [CrossRef]
15. Flerit, F.; Armijo, R.; King, G.C.P.; Meyer, B.; Barka, A. Slip Partitioning in the Sea of Marmara Pull-Apart Determined from Gps Velocity Vectors. *Geophys. J. Int.* **2003**, *154*, 1–7. [CrossRef]
16. Karakaş, Ç.; Armijo, R.; Lacassin, R.; Suc, J.; Melinte-Dobrinescu, M.C. Crustal Strain in the Marmara Pull-Apart Region Associated with the Propagation Process of the North Anatolian Fault. *Tectonics* **2018**, *37*, 1507–1523. [CrossRef]
17. Ambraseys, N.; Finkel, C. Long-Term Seismicity of Istanbul and of the Marmara Sea Region. *Terra Nova* **1991**, *3*, 527–539. [CrossRef]
18. Ambraseys, N.N. The Seismicity of The Marmara Sea Area 1800–1899. *J. Earthq. Eng.* **2000**, *4*, 377–401. [CrossRef]
19. Ambraseys, N.N.; Jackson, J.A. Seismicity of the Sea of Marmara (Turkey) since 1500. *Geophys. J. Int.* **2000**, *141*, F1–F6. [CrossRef]
20. Ambraseys, N. The Seismic Activity of the Marmara Sea Region over the Last 2000 Years. *Bull. Seism. Soc. Am.* **2002**, *92*, 1–18. [CrossRef]
21. Şaroğlu, F.; Emre, Ö.; Kuscu, I. *Active Fault Map of Turkey*; MTA: Ankara, Türkiye, 1992.
22. Stein, R.S.; Barka, A.A.; Dieterich, J.H. Progressive Failure on the North Anatolian Fault since 1939 by Earthquake Stress Triggering. *Geophys. J. Int.* **1997**, *128*, 594–604. [CrossRef]
23. Barka, A. The 17 August 1999 Izmit Earthquake. *Science* **1999**, *285*, 1858–1859. [CrossRef]
24. Reilinger, R.E.; Ergintav, S.; Buergmann, R.; McClusky, S.; Lenk, O.; Barka, A.; Gurkan, O.; Hearn, L.; Feigl, K.L.; Cakmak, R.; et al. Coseismic and Postseismic Fault Slip for the 17 August 1999, M = 7.5, Izmit, Turkey Earthquake. *Science* **2000**, *289*, 1519–1524. [CrossRef] [PubMed]
25. Tibi, R.; Bock, G.; Xia, Y.; Baumbach, M.; Grosser, H.; Milkereit, C.; Karakisa, S.; Zünbül, S.; Kind, R.; Zschau, J. Rupture Processes of the 1999 August 17 Izmit and November 12 Düzce (Turkey) Earthquakes. *Geophys. J. Int.* **2001**, *144*, F1–F7. [CrossRef]
26. Ambraseys, N.N.; Finkel, C.F. The Saros-Marmara Earthquake of 9 August 1912. *Earthq. Eng. Struct. Dyn.* **1987**, *15*, 189–211. [CrossRef]
27. Polonia, A.; Gasperini, L.; Amorosi, A.; Bonatti, E.; Bortoluzzi, G.; Çagatay, N.; Capotondi, L.; Cormier, M.-H.; Gorur, N.; McHugh, C.; et al. Holocene Slip Rate of the North Anatolian Fault beneath the Sea of Marmara. *Earth Planet. Sci. Lett.* **2004**, *227*, 411–426. [CrossRef]
28. Ergintav, S.; Reilinger, R.E.; Çakmak, R.; Floyd, M.; Cakir, Z.; Doğan, U.; King, R.W.; McClusky, S.; Özener, H. Istanbul's Earthquake Hot Spots: Geodetic Constraints on Strain Accumulation Along Faults in the Marmara Seismic Gap. *Geophys. Res. Lett.* **2014**, *41*, 5783–5788. [CrossRef]
29. Yilmaz, Y. Comparison of Young Volcanic Associations of Western and Eastern Anatolia Formed Under a Compressional Regime: A review. *J. Volcanol. Geotherm. Res.* **1990**, *44*, 69–87. [CrossRef]

30. Şimşek, Ş. Geothermal Potential in Northwestern Turkey. In *Active Tectonics of Northwestern Anatolia*; Schindler, C., Pfister, M., Eds.; the Marmara Poly-Project; a Multidisciplinary Approach by Space-Geodesy, Geology, Hydrogeology, Geothermics and Seismology; CHE: Zurich, Switzerland, 1997; pp. 111–123.
31. Hoşgörmez, H.; Yalçın, M.N. Gas-Source Rock Correlation in Thrace Basin, Turkey. *Mar. Pet. Geol.* **2005**, *22*, 901–916. [CrossRef]
32. Pfister, M.; Rybach, L.; Simsek, S. Geothermal Reconnaissance of the Marmara Sea Region (NW Turkey): Surface Heat Flow Density in an Area of Active Continental Extension. *Tectonophysics* **1998**, *291*, 77–89. [CrossRef]
33. Yuce, G.; Italiano, F.; Yasin, D.; Taskiran, L.; Gulbay, A.H. Assessment of the Origin and Geothermal Potential of the Thermal Waters by Hydro-Isotope Geochemistry: Eskisehir Province, Turkey. *Isot. Environ. Health Stud.* **2017**, *53*, 198–211. [CrossRef]
34. Balderer, W.; Greber, E.; Imbach, T.; Rauert, W.; Trimborn, P.; Guler, S. Environmental Isotope Study of Thermal, Mineral and Normal Ground Water within the Bursa and Kuzuluk/Adapazari Areas of Northwestern Turkey. In *Isotope Techniques in Water Resources Development 1991*; IAEA-SM: Vienna, Austria, 1991; pp. 1–4.
35. Greber, E. Deep Circulation of Co2-Rich Paleowaters in Deep Seismically Active Zone (Kuzuluk/Adapazarı, Northwestern Turkey). *Geothermics* **1994**, *23*, 151–174. [CrossRef]
36. Eisenlohr, T. The Thermal Springs of the Armutlu Peninsula (Nw Turkey) and Their Relationship to Geology and Tectonic. In *Active Tectonics of Northwestern Anatolia*; Schindler, C., Pfister, M., Eds.; the Marmara Poly-Project; a Multidisciplinary Approach by Space-Geodesy, Geology, Hydrogeology, Geothermics and Seismology; CHE: Zurich, Switzerland, 1997; pp. 197–228.
37. Pasvanoğlu, S. Hydrogeochemical and Isotopic Investigation of the Bursa-Oylat Thermal Waters, Turkey. *Environ. Earth Sci.* **2011**, *64*, 1157–1167. [CrossRef]
38. Imbach, T. Deep Groundwater Circulation in the Tectonically Active Area of Bursa, Northwest Anatolia, Turkey. *Geothermics* **1997**, *26*, 251–278. [CrossRef]
39. Tut Haklidir, F. Hydrogeochemical Evaluation of Thermal, Mineral and Cold Waters between Bursa City and Mount Uludağ in the South Marmara Region of Turkey. *Geothermics* **2013**, *48*, 132–145. [CrossRef]
40. Yalcin, T. Hydrogeological Investigations of the Gönen and Eksidere Thermal Waters (Nw Turkey). In *Active Tectonics of Northwestern Anatolia*; Schindler, C., Pfister, M., Eds.; the Marmara Poly-Project; a Multidisciplinary Approach by Space-Geodesy, Geology, Hydrogeology, Geothermics and Seismology; CHE: Zurich, Switzerland, 1997; pp. 275–300.
41. Yalcin, T. Geochemical Characterization of the Biga Peninsula Thermal Waters (Nw Turkey). *Aquat. Geochem.* **2007**, *13*, 75–93. [CrossRef]
42. Mutlu, H. Constraints on the Origin of the Balikesir Thermal Waters (Turkey) from Stable Isotope (Delta O-18, Delta D, Delta C-13, Delta S-34) and Major-Trace Element Compositions. *Turk. J. Earth Sci.* **2007**, *16*, 13–32.
43. Sanliyuksel, D.; Baba, A. Hydrogeochemical and Isotopic Composition of a Low-Temperature Geothermal Source in Northwest Turkey: Case Study of Kirkgecit Geothermal Area. *Environ. Earth Sci.* **2011**, *62*, 529–540. [CrossRef]
44. Mützenberg, S. Nature and Origin of the Thermal Springs in the Tuzla Area, Western Anatolia, Turkey. In *Active Tectonics of Northwestern Anatolia*; Schindler, C., Pfister, M., Eds.; the Marmara Poly-Project; a Multidisciplinary Approach by Space-Geodesy, Geology, Hydrogeology, Geothermics and Seismology; CHE: Zurich, Switzerland, 1997; pp. 301–320.
45. Baba, A.; Yuce, G.; Deniz, O.; Ugurluoglu, D.Y. Hydrochemical and Isotopic Composition of Tuzla Geothermal Field (Canakkale-Turkey) and Its Environmental Impacts. *Environ. Forensics* **2009**, *10*, 144–161. [CrossRef]
46. Doğan, T.; Sumino, H.; Nagao, K.; Notsu, K.; Tuncer, M.K.; Çelik, C. Adjacent Releases of Mantle Helium and Soil CO_2 from Active Faults: Observations from the Marmara Region of the North Anatolian Fault zone, Turkey. *Geochem. Geophys. Geosyst.* **2009**, *10*, Q11009. [CrossRef]
47. Géli, L.; Henry, P.; Grall, C.; Tary, J.-B.; Lomax, A.; Batsi, E.; Riboulot, V.; Cros, E.; Gürbüz, C.; Işık, S.E.; et al. Gas and Seismicity within the Istanbul Seismic Gap. *Sci. Rep.* **2018**, *8*, 6819. [CrossRef]
48. Weiss, R. Carbon Dioxide in Water and Seawater: The Solubility of a Non-Ideal Gas. *Mar. Chem.* **1974**, *2*, 203–215. [CrossRef]
49. Holocher, J.; Peeters, F.; Aeschbach-Hertig, W.; Hofer, M.; Brennwald, M.; Kinzelbach, W.; Kipfer, R. Experimental Investigations on the Formation of Excess Air in Quasi-Saturated Porous Media. *Geochim. Cosmochim. Acta* **2002**, *66*, 4103–4117. [CrossRef]
50. White, W.B. Chapter 6—Springwater Geochemistry. In *Groundwater Hydrology of Springs*; Kresic, N., Stevanovic, Z., Eds.; Butterworth-Heinemann: Boston, MA, USA, 2010; pp. 231–268.
51. Giménez, E.; Morell, I. Hydrogeochemical Analysis of Salinization Processes in the Coastal Aquifer of Oropesa (Castellon, Spain). *Environ. Geol.* **1997**, *29*, 118–131. [CrossRef]
52. White, W.M. *Geochemistry*; Wiley-Blackwell: Hoboken, NJ, USA, 2005.
53. Navarre-Sitchler, A.; Thyne, G. Effects of Carbon Dioxide on Mineral Weathering Rates at Earth Surface Conditions. *Chem. Geol.* **2007**, *243*, 53–63. [CrossRef]
54. Stanton, J.S.; Anning, D.W.; Brown, C.J.; Moore, R.B.; McGuire, V.L.; Qi, S.L.; Harris, A.C.; Dennehy, K.F.; McMahon, P.B.; Degnan, J.R.; et al. Brackish groundwater in the United States. In *Professional Paper*; US Geological Survey: Reston, VA, USA, 2017; p. 185. [CrossRef]

55. Rhoades, J.D.; Kandish, A.; Mashali, A.M. The Use of Saline Waters for Crop Production. 1992. Available online: http://www.fao.org/3/a-t0667e.pdf (accessed on 1 February 2025).
56. Balderer, W. Mechanisms and Porcesses of Groundwater Circulation in Tectonically Active Areas. In *Active Tectonics of Northwestern Anatolia*; Schindler, C., Pfister, M., Eds.; the Marmara Poly-Project; a Multidisciplinary Approach by Space-Geodesy, Geology, Hydrogeology, Geothermics and Seismology; CHE: Zurich, Switzerland, 1997; pp. 375–415.
57. Mutlu, H.; Güleç, N. Hydrogeochemical Outline of Thermal Waters and Geothermometry Applications in Anatolia (Turkey). *J. Volcanol. Geotherm. Res.* **1998**, *85*, 495–515. [CrossRef]
58. Ellis, A.; Mahon, W. *Chemistry and Geothermal Systems*; Academic Press: New York, NY, USA, 1977.
59. Bigham, J.M.; Nordstrom, D.K. Iron and Aluminum Hydroxysulfates from Acid Sulfate Waters. *Rev. Miner. Geochem.* **2000**, *40*, 351–403. [CrossRef]
60. Craig, H. Isotopic Variations in Meteoric Waters. *Science* **1961**, *133*, 1702–1703. [CrossRef]
61. Gat, J.R.; Carmi, I. Evolution of the Isotropic Composition of Atmospheric Waters in the Mediterranean Sea Area. *J. Geophys. Res.* **1970**, *75*, 3039–3048. [CrossRef]
62. Hatvani, I.G.; Smati, A.E.; Erdélyi, D.; Szatmári, G.; Vreča, P.; Kern, Z. Modeling the Spatial Distribution of the Meteoric Water Line of Modern Precipitation across the Broader Mediterranean region. *J. Hydrol.* **2023**, *617*, 128925. [CrossRef]
63. Rozanski, K.; Araguás-Araguás, L.; Gonfiantini, R. Isotopic Patterns in Modern Global Precipitation. In *Climate Change in Continental Isotopic Records*; AGU Publications: Washington, DC, USA, 1993; pp. 1–36.
64. Faure, G. *Principles of Isotope Geology*, 2nd ed.; Wiley: New York, NY, USA, 1986.
65. Javoy, M.; Pineau, F.; Delorme, H. Carbon and Nitrogen Isotopes in the Mantle. *Chem. Geol.* **1986**, *57*, 41–62. [CrossRef]
66. Sano, Y.; Marty, B. Origin of Carbon in Fumarolic Gas from Island Arcs. *Chem. Geol.* **1995**, *119*, 265–274. [CrossRef]
67. Italiano, F.; Martinelli, G.; Plescia, P. CO2 Degassing over Seismic Areas: The Role of Mechanochemical Production at the Study Case of Central Apennines. *Pure Appl. Geophys.* **2008**, *165*, 75–94. [CrossRef]
68. Burnard, P.; Bourlange, S.; Henry, P.; Géli, L.; Tryon, M.D.; Natal'in, B.; Sengör, A.M.C.; Özeren, M.S.; Çagatay, M.N. Constraints on Fluid Origins and Migration Velocities Along the Marmara Main Fault (Sea of Marmara, Turkey) Using Helium Isotopes. *Earth Planet. Sci. Lett.* **2012**, *341–344*, 68–78. [CrossRef]
69. Italiano, F.; Martelli, M.; Martinelli, G.; Nuccio, P.M. Geochemical Evidence of Melt Intrusions Along Lithospheric Faults of the Southern Apennines, Italy: Geodynamic and Seismogenic Implications. *J. Geophys. Res. Solid Earth* **2000**, *105*, 13569–13578. [CrossRef]
70. Woith, H.; Zschau, J.; Yilmaz, R.; Karakisa, S.; Zünbül, S.; Baumbach, M.; Grosser, H.; Milkereit, C.; Lang, D.H.; Raschke, M.; et al. Multidisciplinary Investigations of the German Task Force for Earthquakes Related to the Izmit Earthquake of August 17, 1999 and the Düzce Earthquake of November 12, 1999. In *The 1999 Izmit and Düzce Earthquakes: Preliminary Results*; Barka, A., Kozaci, Ö., Ayküz, S., Altunel, E., Eds.; Istanbul Technical University: Istanbul, Türkiye, 2000; pp. 233–245.
71. Italiano, F.; Martinelli, G.; Bonfanti, P.; Caracausi, A. Long-Term (1997-2007) Geochemical Monitoring of Gases from the Umbria-Marche Region. *Tectonophysics* **2009**, *476*, 282–296. [CrossRef]
72. Wang, C.-Y.; Manga, M. New Streams and Springs after the 2014 Mw6.0 South Napa Earthquake. *Nat. Commun.* **2015**, *6*, 7597. [CrossRef] [PubMed]
73. Sato, T.; Kazahaya, K.; Matsumoto, N.; Takahashi, M. Deep Groundwater Discharge after the 2011 Mw 6.6 Iwaki Earthquake, Japan. *Earth Planets Space* **2020**, *72*, 54. [CrossRef]
74. Epstein, S.A.; Mayeda, T.K. Variation of O^{18} Content of Waters from Natural Sources. *Geochim. Cosmochim. Acta* **1953**, *4*, 213–224. [CrossRef]
75. Kendall, C.; Coplen, T.B. Multi-Sample Conversion of Water to Hydrogen by Zinc for Stable Isotope Determination. *Anal. Chem.* **1985**, *57*, 1437–1440. [CrossRef]
76. Yuce, G.; Italiano, F.; D'Alessandro, W.; Yalcin, T.; Yasin, D.; Gulbay, A.; Ozyurt, N.; Rojay, B.; Karabacak, V.; Bellomo, S.; et al. Origin and Interactions of Fluids Circulating over the Amik Basin (Hatay, Turkey) and Relationships with the Hydrologic, Geologic and Tectonic Settings. *Chem. Geol.* **2014**, *388*, 23–39. [CrossRef]
77. Parkhurst, D.L.; Appelo, C.A.J. *User's Guide to Phreeqc (Version 2): A Computer Program for Speciation Batch-Reaction, One-Dimensional Transport and Inverse Geochemical Calculations*; US Geological Survey: Denver, CO, USA, 1999; p. 309.
78. Italiano, F.; Bonfanti, P.; Ditta, M.; Petrini, R.; Slejko, F. Helium and Carbon Isotopes in the Dissolved Gases of Friuli Region (Ne Italy): Geochemical Evidence of Co2 Production and Degassing over a Seismically Active Area. *Chem. Geol.* **2009**, *266*, 76–85. [CrossRef]
79. Italiano, F.; Yuce, G.; Uysal, I.; Gasparon, M.; Morelli, G. Insights into Mantle-Type Volatiles Contribution from Dissolved Gases in Artesian Waters of the Great Artesian Basin, Australia. *Chem. Geol.* **2014**, *378*, 75–88. [CrossRef]
80. Sano, Y.; Wakita, H. Precise Measurement of Helium Isotopes in Terrestrial Gases. *Bull. Chem. Soc. Jpn.* **1988**, *61*, 1153–1157. [CrossRef]

81. Hilton, D.R. The Helium and Carbon Isotope Systematics of a Continental Geothermal System: Results from Monitoring Studies at Long Valley Caldera (California, USA). *Chem. Geol.* **1996**, *127*, 269–295. [CrossRef]
82. Italiano, F.; Martinelli, G.; Nuccio, P.M. Anomalies of Mantle-Derived Helium during the 1997-1998 Seismic Swarm of Umbria-Marche, Italy. *Geophys. Res. Lett.* **2001**, *28*, 839–842. [CrossRef]
83. Pawlewicz, M.J.; Steinshouer, D.W.; Gautier, D.L. Map Showing Geology, Oil and Gas Fields, and Geologic Provinces of Europe Including Turkey. In *Open-File Report*; USGS: Reston, VA, USA, 1997.
84. Stone, J.O.H. Helium Isotopic Tracing of Fluids in the Lithosphere. Ph.D. Thesis, University of Cambridge, Cambridge, UK, 1986.
85. Gülec, N. Helium-3 Distribution in Western Turkey. *Bull. Miner. Res. Explor. Inst. Turk.* **1988**, *108*, 35–42.
86. Imbach, T. Thermalwässer von Bursa. Geologische und Hydrogeologische Untersuchungen am Berg Uludag (Nw Türkei). Ph.D. Thesis, ETH Zürich, Zürich, Switzerland, 1992.
87. Greber, E. Das Geothermalfeld von Kuzuluk/Adapazari (Nw Türkei). Ph.D. Thesis, ETH Zürich, Zürich, Switzerland, 1992.
88. Eisenlohr, T. Die Thermalwässer der Armutlu-Halbinsel (Nw Türkei) und Deren Beziehung zu Geologie und Aktiver Tektonik. Ph.D. Thesis, ETH Zürich, Zürich, Switzerland, 1995.
89. Ercan, T.; Matsuda, J.I.; Nagao, K.; Kita, I. Noble Gas Isotopic Compositions in Gas and Water Samples from Anatolia. In *Geology of the Black Sea Region*; Erler, A., Ed.; MTA: Ankara, Turkey, 1995; pp. 197–206.
90. Gülec, N.; Hilton, D.R.; Mutlu, H. Helium Isotope Variations in Turkey; Relationship to Tectonics, Volcanism and Recent Seismic Activities. *Chem. Geol.* **2002**, *187*, 129–142. [CrossRef]
91. De Leeuw, G.; Hilton, D.; Güleç, N.; Mutlu, H. Regional and Temporal Variations in Co2/He-3, He-3/He-4 and Delta C-13 Along the North Anatolian Fault Zone, Turkey. *Appl. Geochem.* **2010**, *25*, 524–539. [CrossRef]
92. Mutlu, H.; Güleç, N.; Hilton, D.R. Helium-Carbon Relationships in Geothermal Fluids of Western Anatolia, Turkey. *Chem. Geol.* **2008**, *247*, 305–321. [CrossRef]